Automatic adjustment of tire inflation pressure through an intelligent CTIS: Effects on the vehicle lateral dynamic behavior

(Article begins on next page)

08 November 2022

Automatic adjustment of tire inflation pressure through an intelligent CTIS: effects on the vehicle lateral dynamic behavior

d'Ambrosio Stefano[a,*], De Mattei Edoardo[a], Vitolo Roberto[a] and Amati Nicola[b]

(a) Energy Department, Politecnico di Torino, C.so Duca degli Abruzzi 24 - Torino, Italy

(b) Department of Mechanical and Aerospace Engineering, Politecnico di Torino, C.so Duca degli Abruzzi 24 - Torino, Italy

(*) Corresponding Author, email: stefano.dambrosio@polito.it

Abstract

The paper investigates the effect of tire inflation pressure on the lateral dynamics of a passenger car, and presents a possible control-oriented methodology aimed at adapting tire pressure to the current vehicle loading condition targeting a reference characteristic. Starting from the tire characteristics at several inflation pressure levels, the paper investigates the effect of changing selectively tire pressure on each of the two axles, through theoretical calculation of the curvature gain based on the computation of the derivatives of stability, and compares the obtained sensitivity to the results of a multibody simulation model validated through on-track tests. Finally, the work presents a possible algorithm that could be implemented on-board vehicle ECU to provide, for the current loading condition of the vehicle, a tire pressure combination that targets a specific lateral dynamics characteristic. The algorithm is intended as part of the control logic of an intelligent Central Tire Inflation System (CTIS) able to adjust automatically tire pressure according to the actual vehicle working conditions.

1. Introduction

Under-inflated tires are a critical issue for road safety: NHTSA assessed that limiting the maximum tire under-inflation on circulating vehicles to 25% (e.g., thanks to the adoption of Tire Pressure Monitoring Systems – TPMS) would reduce road crashes, avoiding annually 124 fatalities and about 9,000 injuries in the United States [1]. Similarly, it was estimated that incorrect tire pressure causes every year in Europe 35 deaths and more than 4,000 injuries [2]. Furthermore, tire inflation pressure has a direct correlation with tire rolling resistance and is therefore crucial in real-world fuel consumption savings [1,3-8]. On passenger vehicles, a reduction by 25% of tire pressure with respect to the recommended value determines an increment of about 10% in rolling resistance, which leads to a worsening in fuel consumption by 1-2% on a driving cycle, depending on the driving condition [8], and an overall increase in fuel consumption by 1.4% considering an annual driving mission typical for European passenger cars [9], and by 1% on an annual mission typical of the US circulating fleet [10]. The overall impact of tires under-inflation on CO_2 emissions was estimated in 7'290'000 metric tons from the EU fleet [9], and 4'000'000 metric tons from the US fleet [10]. Moreover, incorrect tire pressure produces an improper tread wear and a significant reduction of the tire useful life up to 10-45% if inflation pressure is 0.2-0.6 bar lower than the nominal level [7], which impacts the vehicle cost of ownership [9, 11] and affects environmental sustainability. Concerning the latter topic, on one side, the reduction of tire useful life impacts the volume of used tires to be disposed of at the end of life, and on the other hand, the increase of tire wear leads to a higher amount of particles emitted by the tires and the related pollution due to microplastics [12]. Although not

explicitly mentioned yet by any regulation, PM emitted by the tires represent a relevant topic considering that nowadays about 50% of the PM10 and PM2.5 emissions from vehicle are non-exhaust emissions [13], primarily due to the tires and the brakes [14, 15], and therefore affects vehicles endowed with internal combustion engines as well as electric vehicles [16].

Although tire pressure monitoring systems (TPMS) have been introduced on the market and are nowadays compulsory in Europe, US and other countries [17,18], both indirect and most of the direct TPMSs are able to recognize under-inflation and alert the driver only if the tire pressure is 25-30% lower than the nominal one [1,7]. Nonetheless, such an accuracy of 25-30% cannot be considered acceptable if substantial improvements are targeted. Furthermore, indirect TPMSs have been proved to be ineffective in recognizing low tire pressure in many real-world applications [19]. Moreover, the presence of the TPMS on-board does not provide tires inflated at the correct value since inflation operations are still in charge to the driver himself.

In this scenario, an on-board device able to keep the recommended tire inflation pressure and automatically manage it according to the vehicle current working condition would result in a considerable increase of vehicle road safety and a substantial reduction of real-world fuel consumption [8, 10, 11]. For this purpose, the application of an advanced Central Tire Inflation System (CTIS) to a passenger vehicle and to light and heavy duty commercial vehicles was studied at the Politecnico di Torino by the *Active Tire Pressure Control* (ATPC) team in order to propose some innovative constructive and control solutions [27-29] and assess the potentialities of this technology [8, 10, 11]. The proposed device is intended to adjust tire pressure in order to adapt it to the average working condition during a trip, i.e. the system is actuated at the beginning of a trip in order to adjust tire pressure to the current static vehicle loading conditions, or actuated in the first phases of the trip in order to compensate negative effects of tires cold-start, and then is operated during the trip to maintain the target pressure constant during operation [8]. Therefore, differently from other literature studies which propose an instantaneous tire pressure adjustment [48,49] and a fast-dynamic control of pressure through devices with large volume/weight [49,50], the ATPC team has designed and prototyped a fully integrated and lightweight solution with pneumatic components sized on-purpose in order to obtain a system with a relatively slow actuation dynamics, but still sufficient to obtain significant advantages on fuel economy [10]. Moreover, an active tire pressure control system could be intended as a way to improve vehicle handling through pressure selective management. In particular,

the current paper investigates the potentialities of pressure control as a way to influence vehicle dynamics as the vehicle payload varies.

The tire-road contact patch area, under fixed loading condition, depends on the actual tire inflation pressure. An excessive over-inflation causes a reduction of the contact patch and a consequent reduction of the forces that can be transferred between the tire and the soil. As far as under-inflation is concerned, according to the Pacejka's Magic Formula [20], if the tire pressure is reduced the vertical stiffness decreases so that the tire deflection increases. This determines an increase of tire contact patch [21-24] up to the point in which excessive under-inflation causes an inward deformation of the tread that reduces the contact patch and the traction capability on solid soil, both under dry and wet conditions [22]. The reduction of traction ability and handling is clear when the inward tread deformation occurs. Even if less obvious, low levels of under-inflation can also negatively affect the vehicle dynamics. In this condition, the contact patch area increases (as supported by the evidence of the increase of rolling resistance) but the force per unit area in the footprint (the contact pressure) decreases [1]. In some cases, and especially on wet surfaces, the contact pressure can decrease to a greater extent than the area increase, thus leading to a reduction of the maximum longitudinal and lateral forces that can be transferred to the soil [1]. This can be reasonably related to the variation of the longitudinal, lateral and torsional stiffness with the pressure.

Experimental measurements showed that the effect of tire inflation pressure on both longitudinal and lateral friction coefficients are different for each tire model [24] and can be generalized only in certain ranges, if some approximations are accepted, as in the case of updated versions of Pacejka's Magic Formula or similar models which aim to account for the effect of tire pressure variations [21, 24]. In this paper, the effect of tire inflation pressure on lateral vehicle dynamics has been studied by means of software simulations and experimental tests. The simulations have been performed by means of the software Adams/Car, considering a multibody vehicle model representative of a passenger car. Tire data have been provided by Michelin according to the Pacejka tire model [20]. Experimental on-track tests involved steering pad maneuvers on the reference vehicles/tire combination, at several loading conditions and tire inflation pressures. While previous studies of the ATPC research group at the Politecnico di Torino focused on tire pressure management for the reduction of fuel consumption, the primary aim of this study is to highlight further possible potentialities of tire pressure management in terms of improvements on the vehicle lateral dynamic behavior. Finally, the work presents a methodology for on-board automatic selection of tire pressure aimed at obtaining a target vehicle behavior in terms of vehicle lateral dynamics. Combining this methodology to the evaluation of the effects of tire pressure on fuel

consumption and vehicle longitudinal dynamics (i.e., braking distance) would lead to a decision-making algorithm based on a dynamic multi-objective optimization.

1.1 Active controls on vehicle dynamics: prior art and proposed innovation

Vehicle dynamics control is crucial in case of occurrence of loss of adherence or roll over, which are the conditions where ABS and ESP intervene. Additionally, some technologies have been disclosed to limit the variations of vehicle dynamic behavior from a reference one, such as a real time closed-loop control with a yaw rate controller, based on on-board measurement of the yaw rate [34]. Some electronic controls of vehicle stability that exploit tire-based information have also been described in the technical literature. In example, the actuation of the brakes through the electronic controls (such as ABS, ESP and TCS) could be adapted taking into account the presence of one or more under-inflated tires [35, 36]. Some controls would also require some information related to the specific tire installed on the vehicle, which led to the development of some technologies meant to enable tire-to-vehicle communication to provide tire information to an electronic control unit devoted to the control of vehicle dynamics [37].

An active tire controller device could set different pressure levels according to the driving conditions in order to improve fuel economy on extra-urban driving while prioritizing vehicle dynamics in urban conditions [33]. Also, one or more tires could be quickly deflated in critical situations to reduce stopping distance in emergency braking and to mitigate phenomena such as loss of traction, hydroplaning, oversteering/understeering, etc. [38]. Nevertheless, in the mentioned patents no detail is provided about the method used to evaluate the target inflation values. Moreover, most of the cited examples refer to fast-dynamic controls which intervene on various control parameters to limit the drawbacks in case of occurrence of critical situations.

In the last section of this paper a methodology is presented, which was disclosed in a previous patent application [29], refers to a control that is able to adapt the tire pressure to the current vehicle loading conditions in order to correct the expected vehicle behavior in normal driving conditions and to limit the occurrence of critical situations by means of a pre-arranged adjustment of the vehicle balancing. This is achieved by keeping a desired understeering/oversteering behavior when the vehicle loading condition changes from the reference one. Moreover, different reference understeering/oversteering behavior may be considered according to the surrounding conditions (e.g., weather conditions, soil type, etc…) and achieved by means of the presented methodology.

2. Simulation model and track tests

2.1 Experimental activities on track

Experimental activities were held at the Balocco Proving Ground on the vehicle described in Table 1, thanks to the collaboration with the Vehicle Dynamics laboratory of FCA. Tests were performed by a professional driver, and following all the internal best practices of FCA. Accurate measurement of vehicle speed and angle is obtained through a Corrsys-Datron Correvit S-350 2-axis optical sensor, acquired through a Dewesoft on-board acquisition system. Both the sensor and the acquisition system were provided by FCA, together with the standard instrumentation used to equip the vehicle according to the standard FCA procedures for the tests related to vehicle dynamics. The experimental set-up also included a Stack batteryless TPMS Lite in order to measure the temperature and pressure inside the tires during the maneuvers: the sensors installed inside the tires communicate to the central module via dual-band antennas installed in the wheel-arches, and the acquired signals are then transmitted via CAN to the Dewesoft acquisition device. Furthermore, a Racelogic GPS Sensor VBOX Micro VCI and a Racelogic YAW03 inertial measurement system were installed on-board, and a number of additional signals were acquired from the vehicle CAN line through the OBD port, including the steering-wheel angle, the position of the pedals, engine speed and torque, rotating speed of each wheel, ABS activation signal, etc…

Tests were performed with the vehicle loaded in three different loading conditions (cf. Table 2): the first test case (1350 kg) corresponds to the vehicle equipped with all the instrumentation needed for measurement and acquisition, and with the driver on-board. The other test cases reproduce an intermediate loading condition (1560 kg) and the vehicle maximum payload (1760 kg), and were achieved by loading the vehicle with mannequins on the rear seats and with ballast in the trunk. The vehicle was weighted on balances in the three test conditions before performing the acquisitions, and the detailed weighting conditions for each axle are reported in Table 2, together with the related position of the barycenter. In the three loading conditions, tests were performed with tire pressure equal to 2.3 bar on all tires, evaluated by averaging the pressure measured in each tire along the test maneuvers, after normalizing instant-by-instant the measured pressure to a reference temperature of 25°C. For the baseline loading condition, i.e. 1350 kg, tests were also performed at three different pressure levels, setting the same tire pressure on all the tires.

Vehicle	Fiat Punto MY2012
Engine	Turbo diesel 1248 cc, 62 kW @ 3500 rpm
Transmission	FWD, synchronized MT 5 gears + reverse
Curb weight (nominal)	1145 kg
Brakes Type	Front: disk brakes

Brake modulation	Rear: drum brakes
	ABS
Suspensions	Front: Mc Pherson
	Rear: Torsion bar with interconnected wheels
Geometry	Front overhang: 890 mm
	Rear overhang : 665mm
	Wheelbase: 2510 mm
	Width: 1430 (front) / 1466 (rear) mm
	Height (@ curb weigth): 1490 mm
Tire	185/65 R15 88T

Table 1. Test vehicle data for on-board experimental activity.

Experimental tests were performed in order to characterize the steady-state lateral vehicle dynamic response of the vehicle and consisted in a number of steering pad maneuvers [47]. Among the three possible methods described by the ISO standard (constant-radius, constant steering-wheel angle or constant-speed test methods), the constant-radius test method was adopted, where the vehicle follows a curvilinear trajectory with a constant curvature radius of 40 m and the vehicle speed is increased along the test with an almost-constant gradient. The steering wheel angle is measured by the standard vehicle potentiometer and is acquired via CAN. For each of the testing conditions reported in Table 2, the steering pad maneuver was repeated several times, both in left and right turns. The measurements instruments have different sampling frequencies and CAN output rates. Therefore, each channel was acquired at its maximum frequency and then resampled in post-processing to align sampling frequencies and time scales, and finally filtered with a moving average filter. Data acquired in several repetitions of the same test case where then averaged on a lateral acceleration base: for each test case, each of the relevant variables is divided into lateral acceleration classes with a resolution of 0.01g, and all the data in the same class are averaged, at first averaging among them the repetitions on the same turning verse, and lately averaging the average of all the test repetitions on left turns with the average of all the test repetitions on right turns.

total mass (kg)	1350	1560	1760
mass distribution - Front (%)	63.1	54.6	48.4
mass distribution -Rear (%)	36.9	45.4	51.6
distance of front axle from the barycenter (m)	0.929	1.144	1.300

distance of rear axle from the barycenter (m)	1.590	1.376	1.220

Table 2: loading conditions

2.2 Multibody simulation model

Simulations were performed using the commercial software Adams/Car. As a starting point, a preliminary vehicle model representative of a generic front wheel drive passenger car (B/C segment) was provided by MSC Software. The model is made by several detailed subsystems, such as the chassis, the suspensions, the steering system, etc., interacting through kinematic joints and force elements. The ABS and electronic stability program (ESP) controls are implemented and integrated within the simulation model through the Adams/Mechatronics module. The preliminary model was then adapted to be representative of the geometry, vehicle weight, weight distribution and suspension type of the vehicle described in Table 1.

The results of the track tests described above were used to adapt the preliminary multibody vehicle model to the real vehicle by improving the correlation between the mathematical model and the experimental results.

The comparison among simulations and experimental data was performed in terms of curvature gain K_{RC}, which is used as a parameter representative of the understeering/oversteering characteristic of the vehicle, and is defined as the ratio between the curvature of the vehicle trajectory (1/R) and the steering angle δ (in radians) [30]:

$$K_{RC} = \frac{1}{R\delta}$$ Eq.1

being R the radius of the curvilinear trajectory, which is constant in the case of the steering pad maneuvers described above.

The same steering pad maneuver performed on track was reproduced in the simulation environment. The sensitivity of the curvature gain of the Adams/Car model to changes in suspensions stiffness and preload was studied changing parametrically the two factors on each axle, according to a "one-factor-at-a-time" approach. The test case with the vehicle fully loaded (1760 kg), and with tire inflation pressure equal to 2.3 bar on all the tires was taken as a reference for this sensitivity study. The final settings were chosen as a best-fit of experimental data on this test case. Figure 1 reports the results obtained with the preliminary Adams/Car model and with the updated one for the three load test cases, compared to the experimental results obtained on track. It can be observed that the updated multibody model

provides a good fit to the experimental results at 1560 kg and 1760 kg, while the model did not show any significant improvement with respect to the preliminary one concerning the baseline test case at 1350 kg.

2.3 Tire data and tire model

The reference tire for this study is a 185/65 R15 88T produced by Michelin. Geometrical and experimentally-derived tire data have been provided by the tire manufacturer for this study. Michelin provided the complete characterization according to MF5.2 of the mentioned tire model at three different pressure levels, namely 1.8 bar, 2.2 bar and 2.6 bar. Therefore, the tire is simulated using the Pacejka MF5.2 tire model. This model does not consider the effect of pressure variations on the longitudinal and lateral dynamics nor on the auto-align moment, which was implemented in later versions [21, 24]. Nonetheless, as the data provided by Michelin were derived from experimental tests at the three tire pressure levels, it was preferred to use directly these three datasets for simulations instead than virtually generated datasets to be used with updated tire models which include the tire pressure effect.
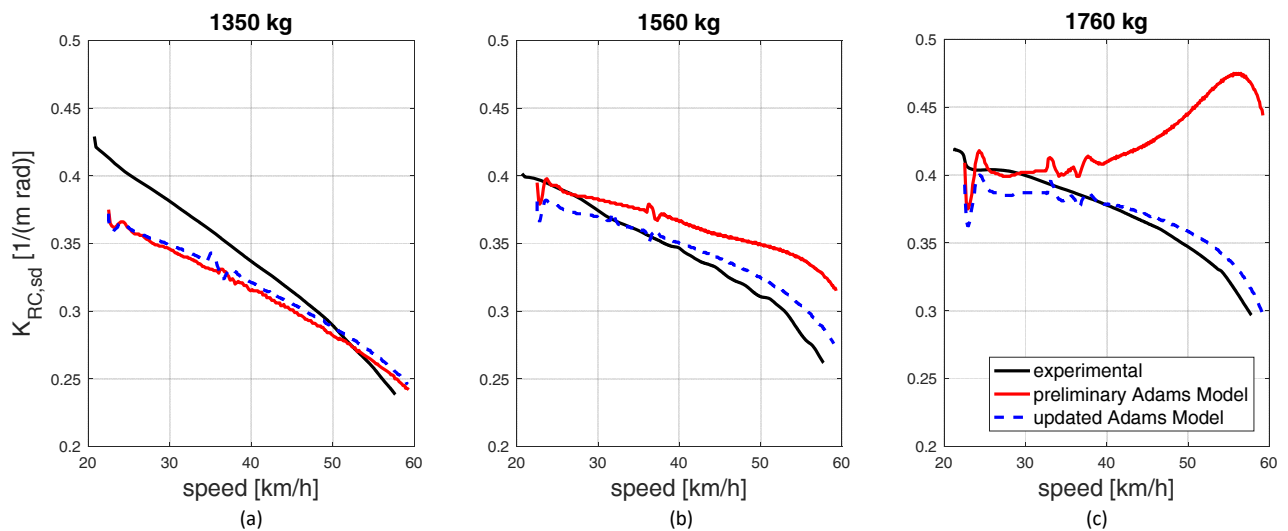

Figure 1 – Comparison of the preliminary Adams/Car model and of the updated one to the experimental results of track tests.

Experimental data refer to tests performed on track with (cold) tire pressure of 2.3 bar on all tires.

3. Effect of inflation pressure on the characteristics of the studied tire

Moving from the datasets available on the reference tire, a preliminary analysis was performed to highlight the effect of tire inflation pressure on the tire characteristic. It is worth to highlight that this effect is known to be tire-dependent, and therefore the comments reported here are not meant as a generalization valid for all the tires.

3.1 Longitudinal dynamics

The Pacejka's tire model for longitudinal dynamics is described by the force coefficient μ_x:

$$\mu_x = \frac{F_x}{F_z}$$

Eq.2

being F_z the vertical force weighting on the tire and F_x the longitudinal force exerted by the tire on the soil, with:

$$F_x = C_\sigma \sigma = 2c_{px}h^2\,\sigma$$

Eq. 3

given a certain longitudinal stiffness coefficient C_σ and being σ the slip ratio, defined as the ratio between the longitudinal velocity of the tire at the contact patch and the longitudinal velocity of the wheel. The longitudinal stiffness coefficient C_σ depends on the square of the contact patch half-length h and on the longitudinal tread stiffness c_{px}.

Figure 2 shows the effect of tire inflation pressure on the longitudinal adherence coefficient μ_x. In Figure 2a the longitudinal adherence vs. slip ratio characteristic is plot for the three levels of pressure and for two loading conditions (the low load condition is plotted in solid lines, the high load in dashed lines), and Figure 2b shows the peak values of the characteristics of Figure 2a. It can be observed that the maximum adherence occurs at the lowest pressure level (1.8 bar), and decreases non-linearly for higher inflation pressures, being negligible the difference between the characteristics at 2.2 bar and at 2.6 bar. Increasing the vertical load acting on the tire reduces the longitudinal adherence, the effect being more evident for slip ratio values higher than 0.1, but the effect of tire pressure is analogous for the two extreme load cases, i.e. the maximum longitudinal adherence is always obtained at 1.8 bar. The longitudinal slip stiffness C_σ resulted to be unaffected by tire pressure, and increases when the vertical load is increased.
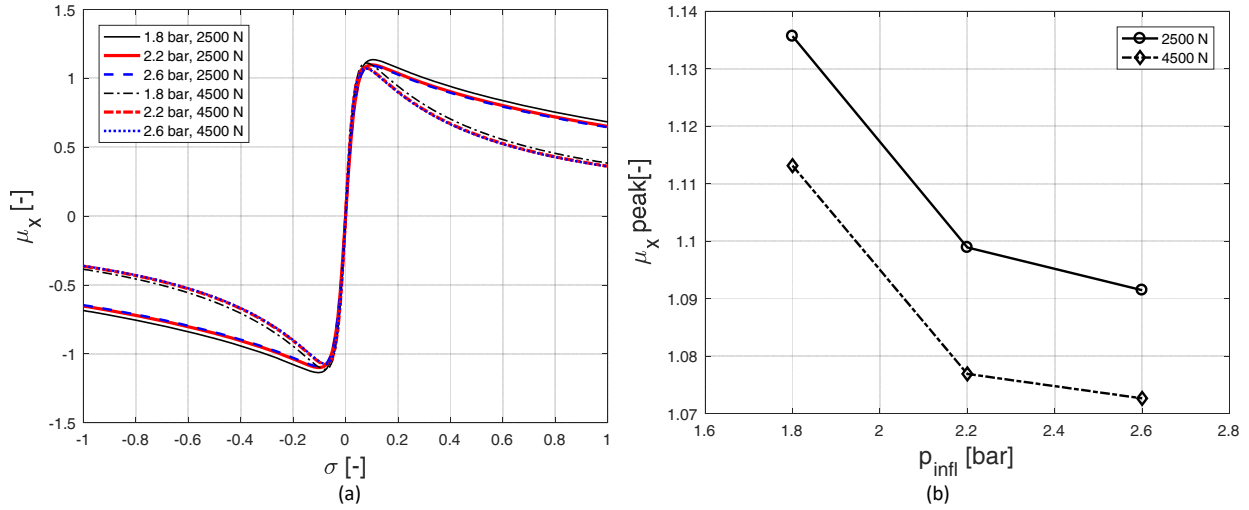
Figure 2 – Effect of tire pressure on longitudinal tire characteristics

3.2 Lateral dynamics

The parameters that mostly influences the lateral dynamics are the lateral friction coefficient μ_y and the cornering

stiffness C_α, defined as

$$\mu_y = \frac{F_y}{F_z}$$

Eq.5

$$C_\alpha = \frac{F_y}{\alpha}$$

Eq.6

where F_y is the lateral force acting at the tire-ground contact and α the side slip angle. According to Pacejka's tire model

[20] the cornering stiffness varies with the vertical load applied to the tire:

$$C_{\alpha(F,R)} = n_w \, PKY1 \, F_{z0} \sin\left[2 \operatorname{atan}\left(\frac{F_{z(F,R)}}{PKY2 \, F_{z0}}\right)\right] \lambda_{Ky\alpha}$$

Eq.7

being n_w the number of wheels per axle, F_{z0} the reference vertical load, $F_{z(F,R)}$ the vertical force acting on the whole

considered axle (the subscript F and R refer to the front and rear axles, respectively), $PKY1$ and $PKY2$ two

experimentally-derived fitting coefficients, and $\lambda_{Ky\alpha}$ a scaling factor which can be used to have a qualitative evaluation

of the effect of changing friction coefficient (e.g., for different grip conditions).

As far as the effect of tire pressure on cornering stiffness is concerned, two different counteracting effects occur. On

one hand, an increase of the vertical stiffness with pressure reduces the contact patch, which is detrimental on the

capacity to transfer forces between the tire and the ground. On the other hand, carcass stiffness also increases with

pressure, therefore carcass deformation decreases and determines an increase of the tread slip angle and of the lateral

force [24]. The two effects have different relative influences under different tire working conditions: the first effect prevails at low vertical loads, while the second is more evident for high vertical loads. In literature, an increased oversteering behavior is highlighted for the underinflated tire [1, 25, 26]: the reduction of lateral stiffness associated with a decrease of the inflation pressure results in a lower cornering force and, as a consequence, in the need for a greater steering angle. Moreover, on a quadruple lane change maneuver the steering effort increases and the maximum absolute value of the vehicle slip angle increases if the pressure is decreased in all the tires [26], and a further increment of the vehicle slip angle (i.e., a more oversteering behavior) is obtained if only rear tires are deflated while a more understeering behavior derives from a reduction of the inflation pressure of the front tires only. This effect is also dependent on the loading condition, both in terms of vehicle mass and center of gravity (CoG) position.

Figure 3 reports the lateral characteristics of the tire for the three levels of tire inflation pressure. Lateral adherence results to be larger at lower pressure levels (Fig. 3a,b), being in this case the effect of tire pressure almost linear on the peak lateral adherence coefficient, and larger at lower vertical load (Fig. 3b). When the tire is loaded with low vertical loads, also cornering stiffness decreases with an increase in tire inflation pressure (cf. Fig. 3d), while the effect of tire pressure on cornering stiffness is opposite when the tire is loaded with the maximum vertical force. With reference to Fig. 3c, in fact, at low loads the cornering stiffness increases linearly with vertical load and is larger at lower inflation pressure: in this condition, the variation of the vertical stiffness of the tire – which generates the increase of the contact patch area with lower tire inflation pressure – is prevailing over the variation of the carcass stiffness [24]. On the other hand, at higher vertical loads, the increase of the carcass stiffness for higher inflation pressures dominates over the variation of the contact patch area, thus leading to a higher cornering stiffness with higher tire inflation pressure. The characteristics show a cross-point around 3200 N. The sensitivities of the cornering stiffness to vertical load and tire pressure are also reported in Figure 3e in the form of a contour plot.

Still with reference to Figure 3c, some further considerations are possible by taking into account the influence of the cornering stiffness on the understeering coefficient, where the understeering coefficient can be defined as [30]:

$$K_{US} = \frac{mg}{w_b^2}\left(\frac{w_b - x_F}{C_{\alpha F}} - \frac{x_F}{C_{\alpha R}}\right)$$

Eq.8

being w_b the wheelbase, x_F the distance between the vehicle barycenter and the front axle, m the vehicle mass in a generic vehicle loading condition, g the gravitational acceleration, and being $C_{\alpha F}$ and $C_{\alpha R}$ the front and rear cornering stiffness, respectively, according to Eq.7. The understeering coefficient, as defined in the equation above, is reported in

Figure 4 in the form of a contour plot as a function of the cornering stiffness of the front and rear axles, for the two extreme loading conditions of Table 2.

Therefore, in a low-load condition (i.e., vertical load on all the tires lower than the cross-point) an increase of tire pressure only on front tires would lead to a reduction of the front cornering stiffness $C_{\alpha F}$, thus increasing the understeering coefficient, and – on the other hand - a pressure increase on rear tires only would reduce the rear cornering stiffness $C_{\alpha R}$ thus making the vehicle more oversteering (i.e., reducing the understeering coefficient). The effect instead becomes opposite for loads bigger than the one corresponding to the cross-point of the characteristics. The effect is obviously bigger in vehicles subjected to great load changes like trucks and buses as it was experimentally observed by Fancher [31] and by Al-Solihatet al. [32], and specifically depends on the sensitivity of each specific tire model to pressure changes.

3.3 Self-aligning moment

Finally, with reference to Figure 5a, the dependence of the self-aligning moment on tire pressure is reported, where the self-aligning moment M_z is defined as:

$$M_z = F_y t = C_{\alpha,M_z}\alpha \qquad\qquad\qquad \text{Eq.9}$$

where t is the pneumatic trail, i.e. the distance between the center of the contact patch and the point where the resultant of side forces, F_y, is applied, and C_{α,M_z} is the aligning stiffness [20].

The graphs show that the self-aligning moment, decreases increasing the inflation pressure and increases increasing the load. The aligning moment stiffness (Figure 5b,c), evaluated as the slope in the origin of the curves of Figure 5a, also increases almost linearly with an increase of pressure and it is larger increasing the vertical load on the tire.
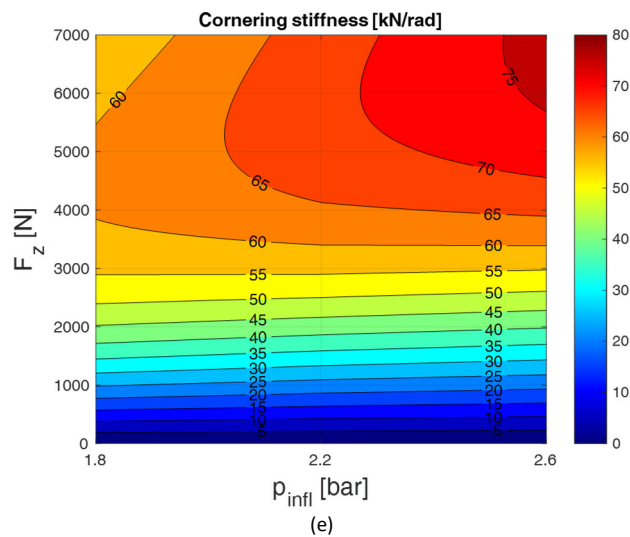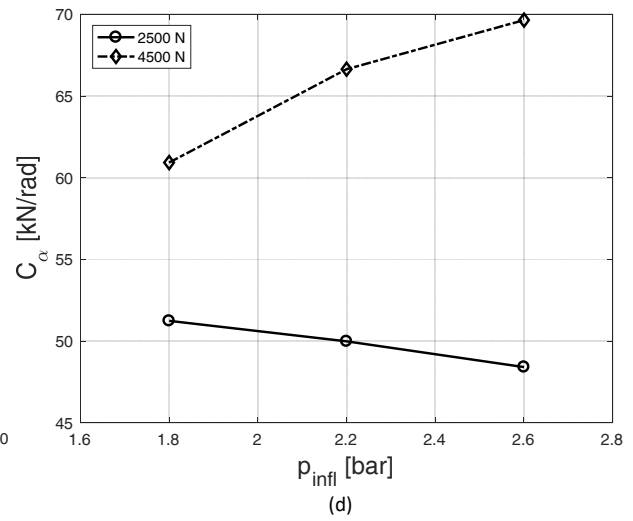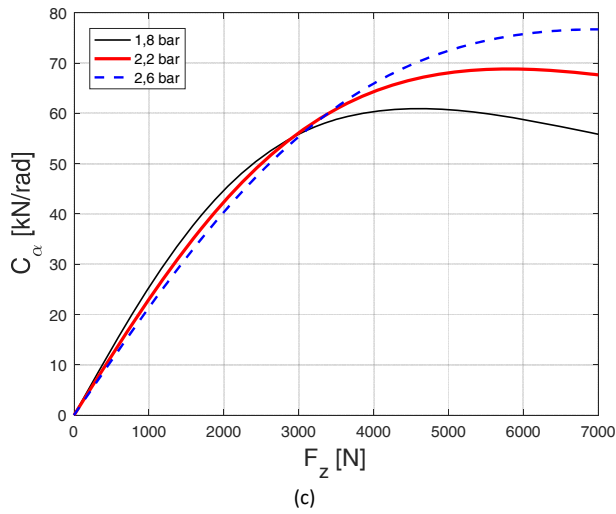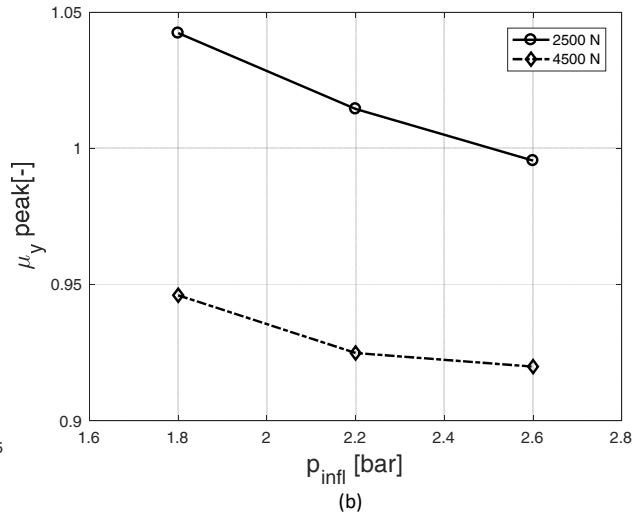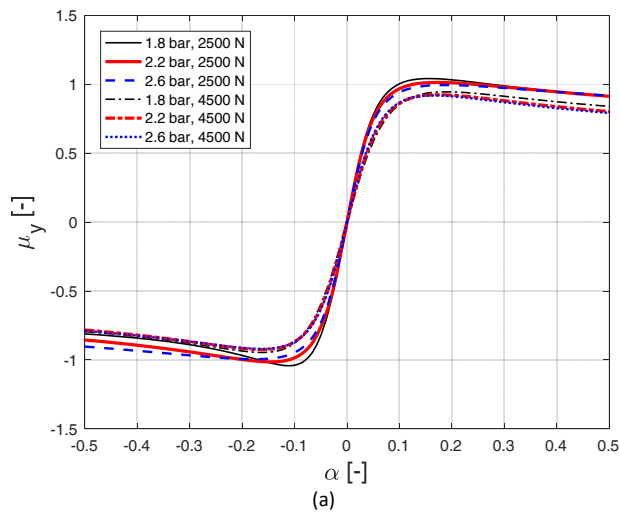
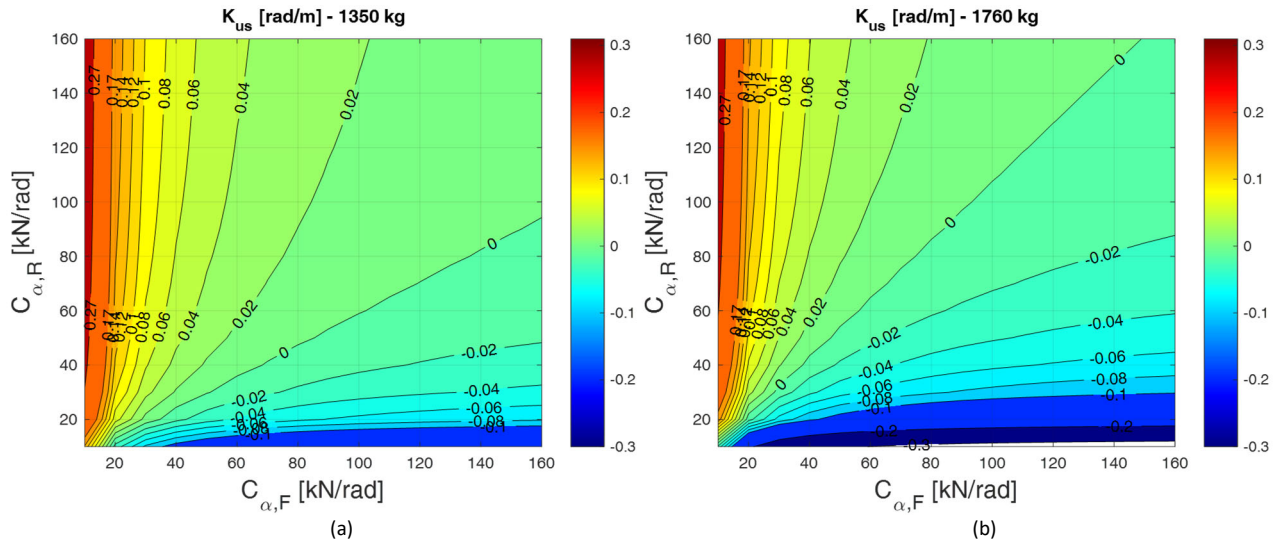*Figure 3 – Effect of tire pressure on lateral tire characteristics.*

Figure 4 – Understeering coefficient K_{US} ae defined in Eq.8 as a function of the total front and rear axles cornering stiffness, in two loading conditions: 1350 kg (a) and 1760 kg (b) of total vehicle mass.

4. Effect of tire inflation pressure and vehicle loading condition on lateral vehicle dynamics

Lateral vehicle dynamics was studied through experimental tests and simulation work in order to evaluate the effect of a variation in the vehicle loading condition and of tire inflation pressure on the understeering/oversteering behavior of the vehicle.

4.1 Theoretical curvature gain

As already mentioned, this comparison focuses on the curvature gain characteristic, where the curvature gain introduced in Eq. 1 is defined by means of a simplified bicycle model as [30]:

$$K_{RC,K} = \frac{1}{R\delta} = \frac{1}{w_b\left(1+K_{US}\frac{v^2}{g\,w_b}\right)}$$

Eq.10

being K_{US} the understeering coefficient defined in Eq. 8 and v the vehicle speed. This definition of the curvature gain is identified in this paper with the subscript "K", which stands for "kinematic".
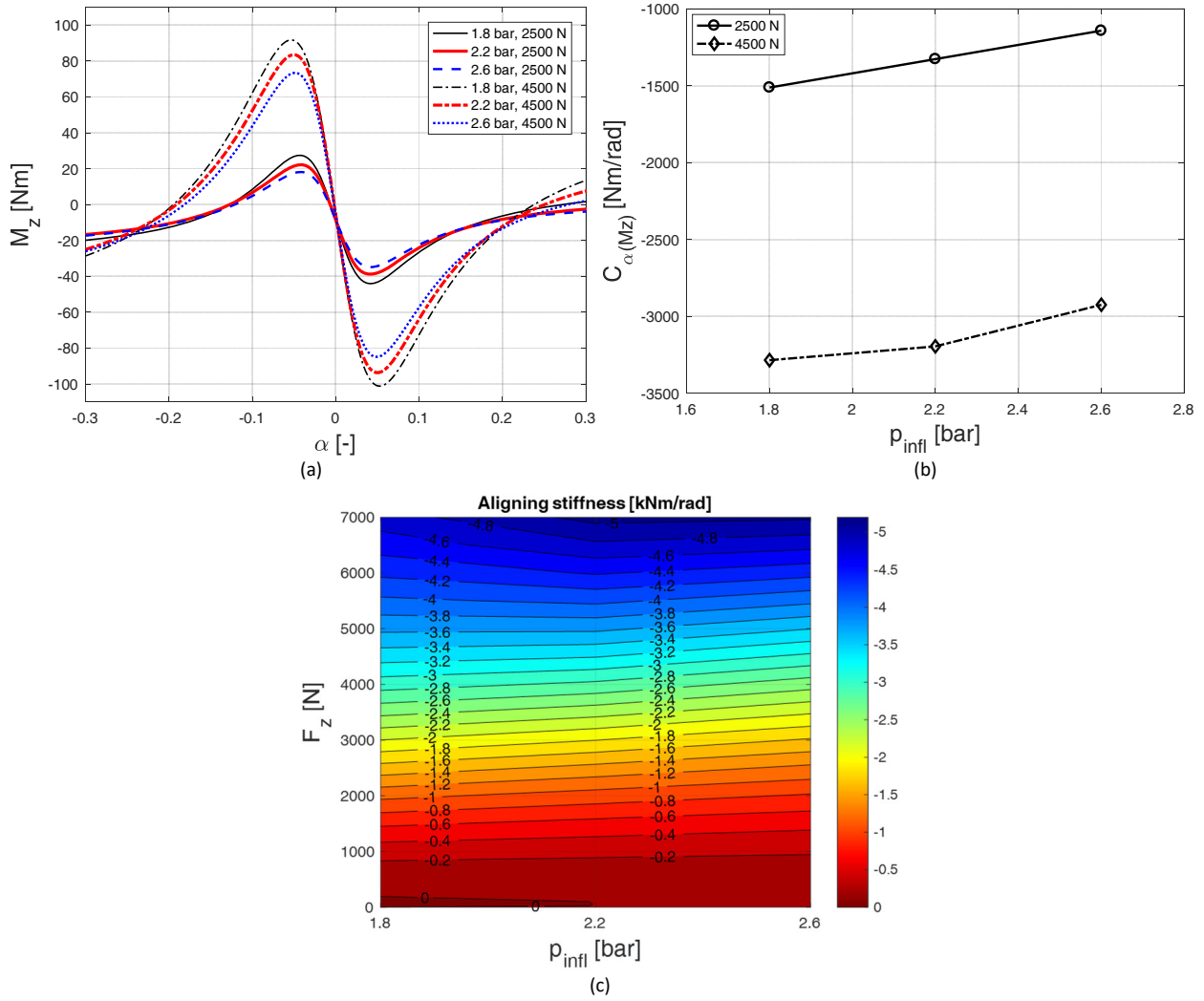
Figure 5 – Effect of tire pressure on self-aligning moment.

A more accurate estimation of the curvature gain can be obtained through the so called stability derivatives, which represent the derivatives of the lateral force and yawing moment with respect to the side slip angle β of the vehicle, the yaw angular velocity r and the steering angle δ, and can be obtained according to different assumptions. Typically, two models are used: the first, also referred as "low speed cornering" model, is based on the assumption of steady state cornering (constant path curvature) and on which only cornering forces acting on the tire are considered; the latter, also referred as "high speed cornering" model, neglects the interaction between longitudinal force and lateral force but considers the effect of the self-align torque. In this work, the used definition of curvature gain evaluated through the stability derivatives, indicated with the symbol $K_{RC,sd}$ always refer to the "high speed cornering" model, whose definition as retrieved from [30] is reported in the following Equation:

$$K_{RC,sd} = \frac{1}{R\delta} = \frac{N_\beta Y_\delta - N_\delta Y_\beta}{v[N_\beta(mv - Y_r) + N_r Y_\beta]}$$

Eq.11

which is obtained from the definition of curvature gain (Eq.1) through the application of the equations of motion of the vehicle under steady state conditions. The terms Y_β, Y_r and Y_δ in Eq.11 represent the derivatives of the side force F_y with respect to the three components β, r and δ, and the terms N_β, N_r and N_δ, similarly, represent the derivatives of the yawing moment M_z with respect to β, r and δ. These terms can be defined from the linearization of F_y and M_z and, according to the procedure demonstrated by Genta et al. in [30], the following formulations can be obtained:

$$Y_\beta = -\sum C_{\alpha(i)} + \frac{1}{2}\rho v_r^2 S (C_y)_\beta \qquad \text{Eq.12}$$

$$Y_r = -\frac{1}{v}\sum x_i C_{\alpha(i)} \qquad \text{Eq.13}$$

$$Y_\delta = \sum (C_{\alpha(i)} + F_{x_i}) K_i' \qquad \text{Eq.14}$$

$$N_\beta = \sum [-x_i C_{\alpha_i} + (M_{z_i})_\alpha] + \frac{1}{2}\rho v_r^2 S (C_{M_z})_\beta \qquad \text{Eq.15}$$

$$N_r = -\frac{1}{v}\sum \left[-x_i^2 C_{\alpha_i} + (M_{z_i})_\alpha x_i \right] \qquad \text{Eq.16}$$

$$N_\delta = \sum \left[C_{\alpha_i} x_i - (M_{z_i})_\alpha + F_{x_i} x_i) \right] K_i' \qquad \text{Eq.17}$$

being:

- C_{α_i} is the cornering stiffness of the i-axle;

- $(M_{z_i})_\alpha$ is the ratio between the self-align torque M_z of the i-axle and the side slip angle α and it is defined according to Pacejka tire model as

$$(M_{z_i})_\alpha = F_{z_i} \left(\frac{R_{ul}}{F_{z0}} \right) \left(QDZ1 + QDZ2 \frac{F_{z_i} - F_{z0}}{F_{z0}} \right) \lambda_t \, \text{sgn}(v_x) \, C_{\alpha_i} \qquad \text{Eq.18}$$

being QDZ1 and QDZ2 two experimentally-derived coefficients, λ_t the scale factor of peak pneumatic trail (usually equal to 1), R_{ul} the tire unloaded radius, v_x the longitudinal tire speed at which the tire coefficients have been calculated and where the contribution due to QDZ2 is neglected in most of the practical applications;

- x_i is the distance of the i-axle from the center of gravity;

- v_r is the radial vehicle speed;

- ρ is the density of the ambient air;

- S is the frontal area of the vehicle;

- $(C_y)_\beta$ is the ratio between the lateral aerodynamic coefficient Cy and the sideslip angle β of the vehicle;

- $(C_{M_z})_\beta$ is the ratio between the aerodynamic coefficient relative to the yaw moment and the sideslip angle β of the vehicle;

- F_{x_i} the longitudinal force, where all the terms F_{x_i} are usually neglected;

- K'_i is equal to 1 for the steering axle and null on the non-steering axle(s) in a vehicle with only one steering axle.

The subscript *i* identifies each of the axles of the vehicle, and corresponds to the subscripts *F* and *R* (front or rear, respectively) in the case of a two-axle vehicle.

Stemming from the data available for the abovementioned tire and vehicle, the curvature gain has been calculated for various loading conditions, including those reported in Table 2, and for the three pressure levels at which tire characterization was available. The results are reported in Figure 6.

Figure 6a reports the variation of the understeering characteristic with a change in the loading condition of the vehicle and a change in tire inflation pressure, with tire pressure equalized among the tires. In the graph, each color and symbol refers to a loading condition, while different line styles refer to different tire pressure combinations. For a given level of pressure, e.g. 2.2 bar (dashed lines in Fig. 6a), it can be observed that the vehicle becomes less understeering as the load is increased. Moreover, it can be observed that at the lower loading cases (1350 kg and 1560 kg, black lines with square markers and red lines with cross symbols, respectively) a lower tire pressure leads to a more understeering behavior of the vehicle. For the higher loading condition (1760 kg, blue lines with circles) a change in tire pressure produces only a small effect on the understeering characteristic if the pressure is equalized on the four tires, the lower tire pressure (1.8 bar) leading to a slightly less understeering behavior (i.e., a curvature gain with a negative gradient with lower absolute value) with respect to keeping the tires inflated at 2.2 bar or 2.6 bar. It is worth to notice that the load distributions measured experimentally on the balances before the on-track tests for all the measured conditions was considered in the calculations, with the barycenter of the vehicle moving backward as the payload increases.
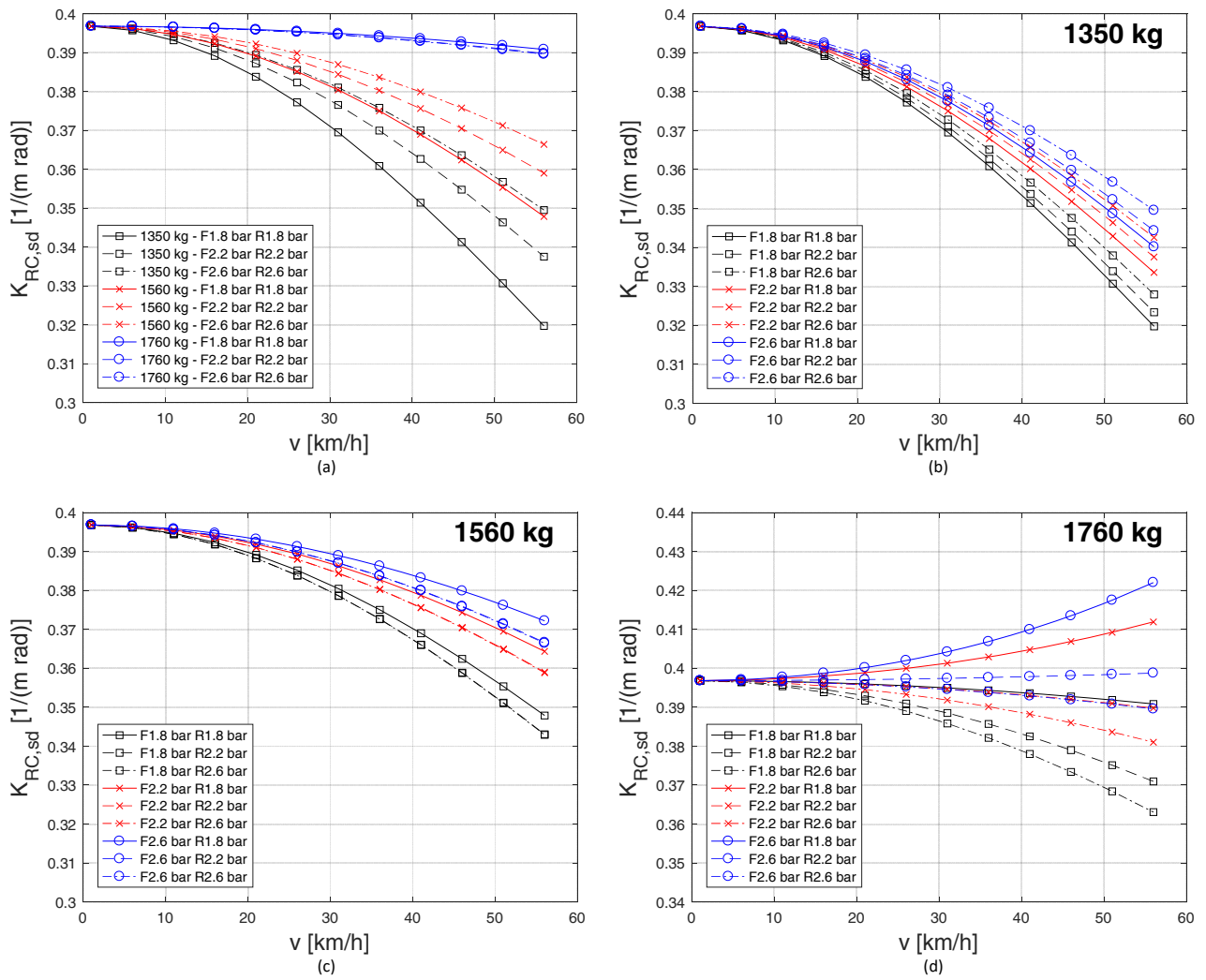
Figure 6: Theoretical curvature gain for the vehicle-tire combination on Table 1: effect of vehicle load and tire pressures.

Figures 6b-d report the effect of changing tire pressure individually on each axle, and each graph refers to a different loading condition. In these graphs, each combination of color and symbol refers to a certain inflation pressure on the front axle, i.e. 1.8 bar (black lines with square markers), 2.2 bar (red lines with cross symbols) and 2.6 bar (blue lines with circles), while line styles identify the tire pressure on the rear axle (solid line for 1.8 bar, dashed line for 2.2bar, dashed-dotted line for 2.6 bar).

It can be observed that for the baseline loading condition (1350 kg, Fig. 6b) increasing tire pressure on the rear axle leads to a less understeering behavior for all the tire pressure levels set on the front tires, while for the other considered loading cases (1560 kg, Fig.5c and 1760 kg, Fig. 6d) the opposite effect is observed, i.e. increasing tire pressure on rear tires leads to a more understeering behavior. Increasing tire pressure from 2.2 bar to 2.6 bar only on the rear axle has a negligible effect at 1560 kg (notice that the two characteristics are overlapped in the graph). Furthermore, an increase of tire pressure only on front tires leads to a less understeering vehicle at the reference loading case (Fig. 6b), while it

leads to a more oversteering vehicle for the cases with higher payload. Some cases are highlighted where the vehicle becomes critically oversteering at 1760 kg, when tire pressure is lower on rear tires than on front ones.

4.2 Multibody simulations: step steer maneuver

Several simulations were performed through the multibody vehicle model described in Section 2, for the three loading conditions reported in Table 2, and varying tire pressure. In the following, only the two extreme loading cases will be presented for the sake of brevity. The simulations included both a step steer maneuver and a steering pad test.

The step steer maneuver consists in a "step input" provided to the steering wheel while the vehicle is running at constant speed. In detail, in the simulated maneuver the vehicle is run at 70 km/h and then (2 seconds after the beginning of the simulation time) a steering wheel input is provided with an angle of 30° and a gradient of 200°/s, which is then maintained constant.

In Figure 7, the cornering stiffness of the tires is plotted, which was already discussed in Figure 3c. In Figure 7, anyway, also the vertical load acting on each tire during the second phase of the maneuver (after the application of the steering input) is reported for the two loading cases described hereinafter.

Referring to the first loading case (1350 kg, Fig. 7a), an increase of tire inflation pressure on the rear axle generates a decrease in the cornering stiffness while on front tires the opposite trend occurs as the vertical load on both the wheels is higher than the cross-point among the characteristics. Therefore, according to Eq.8, it is expected that an increase of tire pressure on any of the two axles would reduce the understeering coefficient. Figure 8 reports the result of the step steer maneuver for the loading case 1350 kg, in terms of lateral acceleration in time (Fig. 8a) and in terms of acceleration gain (Fig. 8b) ${a_{y,st}}/{\delta}$, where the acceleration $a_{y,st}$ is the steady lateral acceleration in the second phase of the maneuver. It can be observed that both an increase of tire pressure on the front and/or on the rear tires produces an increase of the lateral acceleration (in absolute terms) and of the acceleration gain, i.e. an increase of the oversteering tendency of the vehicle.
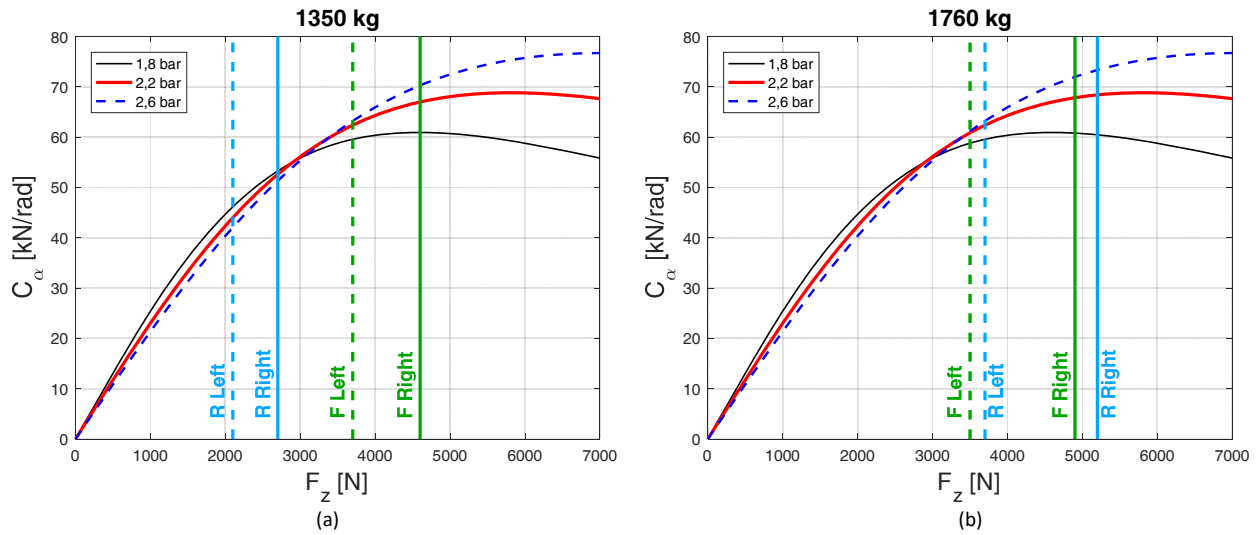
Figure 7: Cornering stiffness vs. vertical load at various inflation pressures: evidence on the vertical load acting on each tire during the studied maneuver for the loading case 1350 kg (a) and 1760 kg (b).
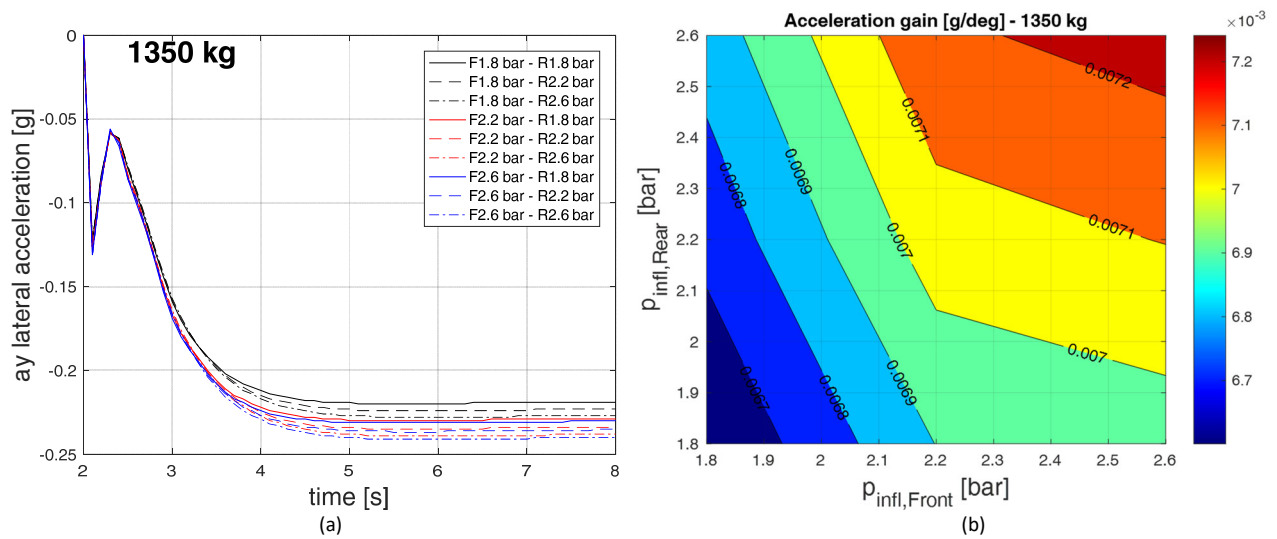

Figure 8: Step steer maneuver in Adams/Car: lateral acceleration profiles in time (a) and acceleration gain in the final steady part of the maneuver (b) for the loading case at 1350 kg.

With reference to Figure 7b, for the loading case 1760 kg it can be observed that all the wheels are loaded at a vertical force higher that the cross point among the characteristic: an increase of tire pressure on any axle leads to an increase of the cornering stiffness on front tires. For the front axle, it would lead to an increase of the oversteering tendency of the vehicle. On the other hand, an increase of tire pressure on rear tires would lead to an increase of the understeering tendency of the vehicle. Figure 9 shows the results of the simulations for this loading condition: increasing tire pressure

only on the rear axle leads to a reduction of the lateral acceleration and of the acceleration gain (being the steering angle constant the lateral acceleration and the acceleration gain are proportional to each other). On the other hand, increasing tire pressure on the front axle only leads to an increase of the lateral acceleration. The minimum steady lateral acceleration is obtained when tire pressure is set at 1.8 bar on the front tires and at 2.6 bar on the rear ones, which is therefore the condition that leads to an higher understeering tendency of the vehicle, while – in accordance with what discussed from the results of the calculation of the theoretical curvature gain - the highest lateral acceleration is obtained when tire pressure is set to 2.6 bar on the front tires and to 1.8 on the rear ones.
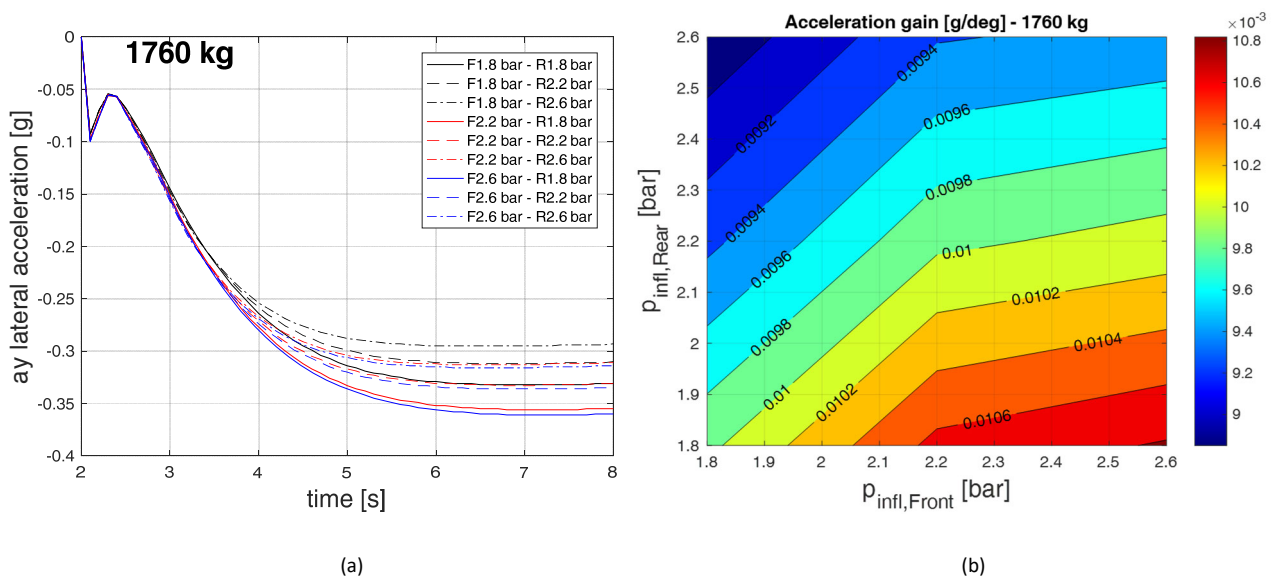

Figure 9: Step steer maneuver in Adams/Car: lateral acceleration profiles in time (a) and acceleration gain in the final steady part of the maneuver (b) for the loading case at 1760 kg.

In order to also highlight the effect of the tire pressure during the first part of the maneuver, just after the input on the steering wheel, in Figure 10 is also reported the peak values of the acceleration peak in the first part of the maneuver, i.e. the relative minimum visible in Figures 8a and 9a about 0.2s after the beginning of the maneuver, mapped as a function of front and rear tire pressure for the two loading conditions of Figs. 8 and 9. It is highlighted that in both the loading conditions an increase of front tire pressure results in an increase of the absolute value of the acceleration, while an increase in rear tire pressure slightly reduce the acceleration amplitude in low load-low pressure conditions (left-hand part of Figure 10a), and has the opposite effect on the high load-high pressure cases (right hand part of Figure 10b). The effect of tire pressure on the peak transient acceleration is generally small.

4.3 Multibody simulations: steering pad maneuver

The steering pad maneuver was also tested in the Adams/Car simulation environment, where the curvature radius R was 40 m (as for the experimental tests on track), and the maneuver simulated an increase of lateral acceleration from 0.1g to 0.7g. The results are reported in Figure 11 for the 1350 kg loading case and in Figure 12 for the 1760 kg condition, and expressed in terms of the curvature gain, which was calculated according to Eq. 1 through the steering angle resulting from the simulations. Coherently with the theoretical calculations of the curvature gain and with the step steer multibody simulations, also for this maneuver it was found an increase of the curvature gain (i.e., a reduction of the understeering tendency of the vehicle) when both front and rear tire pressure are increased if the vehicle is in a low-load condition (Fig. 11), while at full-load (Fig. 12) the vehicle becomes more oversteering if the pressure is increased on the front tires, and more understeering if the pressure is increased on the rear tires. Generally, the vehicle results in a higher oversteering tendency when the payload is higher. Figures 11b and 12b also report the contour plot of the curvature gain values obtained at 50 km/h as a function of front and rear tire pressure: it is highlighted that the trend with pressure of the curvature gain estimated from the steering pad maneuver is the same already shown for the acceleration gain evaluated on the step steer maneuver (Figs. 8b and 9b).

4.4 Results of track tests

Some tests were performed on track in order to confirm the change in the understeering behavior of the vehicle predicted through the calculation of the stability derivatives and also shown by simulations. Steering pad tests were performed for the three loading conditions reported in Table 2 at the reference tire inflation pressure of 2.3 bar (cf. Figure 13a) and for three pressure levels for the reference loading case (cf. Figure 13b). Experimental data were processed as mentioned in Section 2, and the results are reported in Figure 10 in terms of curvature gain vs. vehicle speed. The experimental results thus confirm the theoretical calculations of the curvature gain, showing a reduction of the understeering when the vehicle mass is increased with constant tire inflation pressure, and a reduction of the understeer when tire pressure is increased on the four tires when the vehicle is in the reference loading condition of 1350 kg.
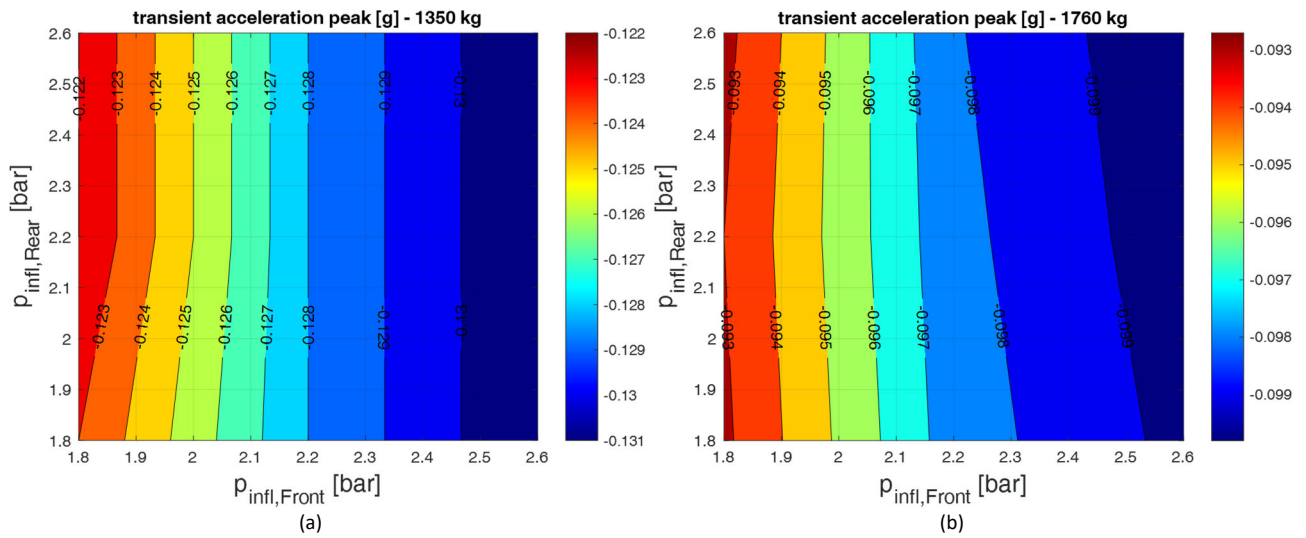
Figure 10: Step steer maneuver in Adams/Car: peak transient acceleration as a funtion of front and rear tire pressure at 1350kg (a)
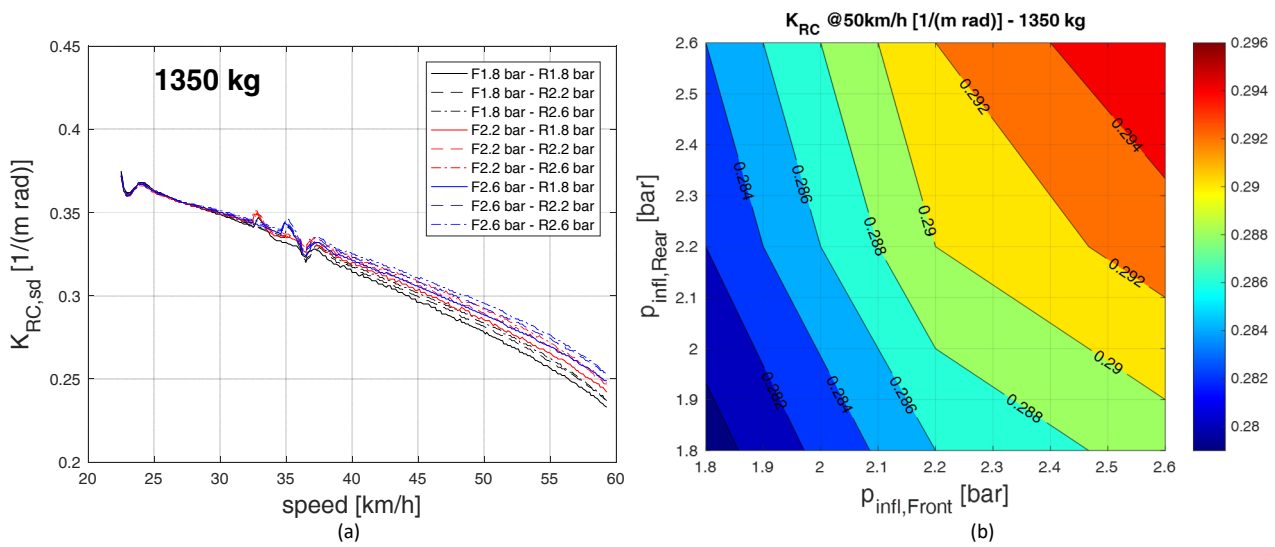
and 1760 kg (b).

Figure 11: Curvature gain on the steering pad maneuver in Adams/Car with the vehicle loaded at 1350 kg.
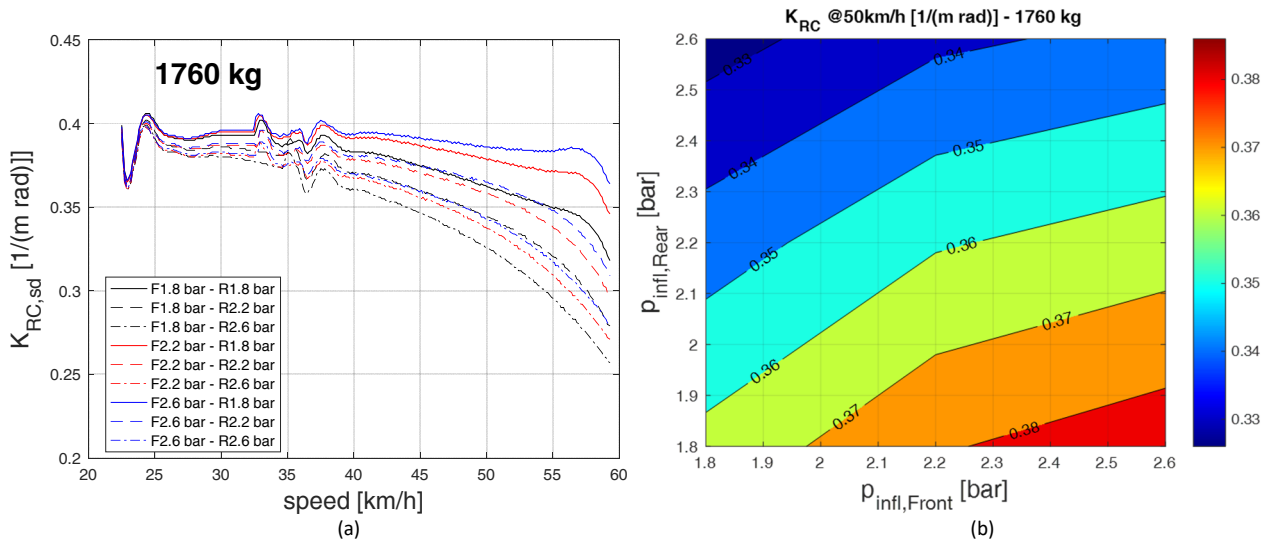
Figure 12: Curvature gain on the steering pad maneuver in Adams/Car with the vehicle loaded at 1760 kg.
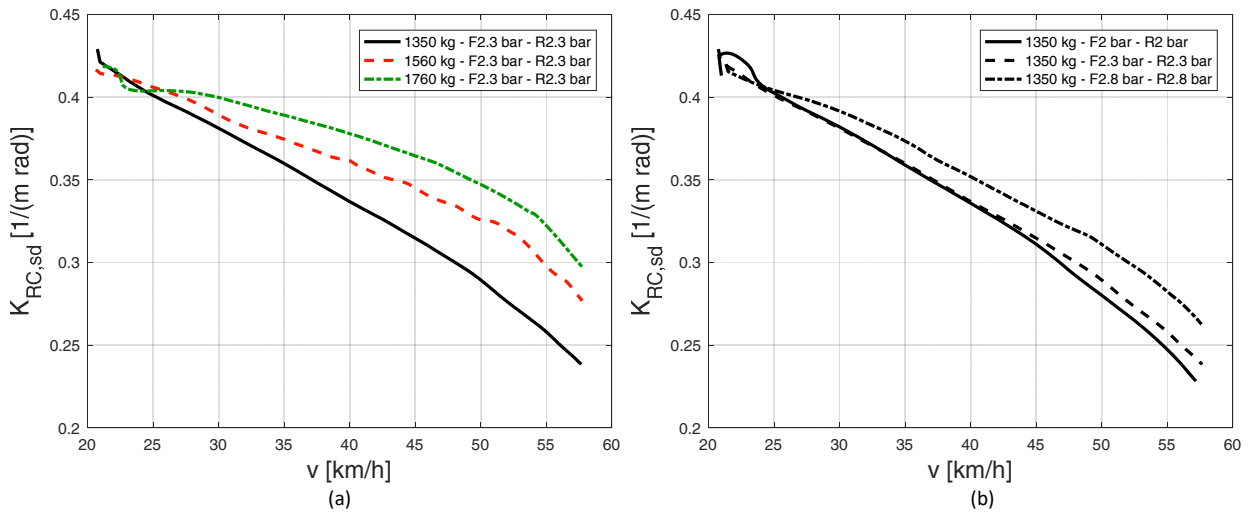
Figure 13: Results of steering pad maneuvers performed at the Balocco Proving Ground: effect of loading conditions at reference tire pressure (a) and effect of changing tire pressure for the baseline loading condition (1350 kg) with tire pressure equalized on the four wheels (b).

5. Adjusting tire inflation pressure with vehicle loading condition

From the study discussed above, it is evident – and it is also qualitatively known in terms of common knowledge – that a change in the loading condition of the vehicle determines a variation on the vehicle lateral dynamic characteristics, and that the understeering/oversteering behavior of the vehicle is also affected by tire inflation pressures. Usually, the car manufacturers provide a "nominal" tire inflation pressure in reference vehicle loading conditions, i.e. a compromise level that can provide an acceptable performance in each vehicle working condition taking into account vehicle

longitudinal and lateral dynamics as well as fuel consumption. Moreover, some prescriptions may be suggested by the car makers about how to adjust the inflation pressure to adapt the tire to the vehicle load. Nevertheless, tires characteristics and their sensitivity to a change in tire pressure are different for different tire models. Moreover, often the drivers do not control or adjust frequently tire pressures, e.g. vehicles are typically run at a fixed tire pressure for all the working conditions.

Therefore an advanced Central Tire Inflation System (CTIS), able to manage autonomously tire inflation pressure by means of proper automatic inflation and deflation operations, can be intended as an active control which could provide benefits by means of the adaption of tire pressure to the current vehicle working conditions. More in detail, an intelligent CTIS could set the tire inflation pressure in order to improve fuel economy and/or vehicle handling having in input proper parameters that describe the vehicle state. Seymour et al. [33] presented the possibility to have such an intelligent control, where various parameters – including ambient conditions, loading conditions, vehicle speed, engine fuel flow rate, brake pedal, GPS, navigator, etc… – are used as input for the CTIS electronic control unit, but in the mentioned patent an algorithm is not explicitly described to select tire pressure according to these parameters.

The ATPC team at the Politecnico di Torino has been working on the development of an automatic central tire inflation system, aiming at an autonomous management of the tire pressure on board through the definition of rule-based strategies to be implemented in the control unit of the CTIS. Some of the proposed strategies are focused on the reduction of fuel consumption and were presented and discussed in previous works [8- 11]. The current paper focuses on the definition of a methodology to choose tire inflation pressure according to the current vehicle loading conditions to obtain a target understeering/oversteering behavior for a certain vehicle-tires combination. The methodology is meant to be developed as an algorithm to be implemented on-board as part of the control logic of an intelligent CTIS. On the other hand, if a CTIS is not present on-board, the output of this algorithm could be used to suggest to the driver the proper tire pressure to be set in the current working conditions, e.g. through the on-board computer, or through a mobile application.

5.1 Calculation of target tire pressure with different loading conditions: methodology

Stemming from the knowledge of the current loading condition of the vehicle and from a quantification of the effect of tire pressure on the tire characteristics, it is possible to calculate the understeering characteristic of the vehicle at the current loading condition for several combinations of tire pressures, according to the methodology presented in a

previous patent application [29] and briefly presented herein after. As shown in Figure 5, this can be obtained, in example, through the computation of the theoretical curvature gain vs. vehicle speed, calculated through any of the two formulations reported in Eq. 10 and Eq. 11. A reference curvature gain characteristic could also be defined, as the curvature gain calculated in a reference loading condition and with a reference combination of tire pressures. Finally, the tire pressure to be set for the current loading condition can be obtained comparing – through some maximum like-hood methodology – the curvature gain characteristics obtained for several tire pressure combinations at the current loading conditions with the reference one. The tire pressure combination that provides the curvature gain most similar to the reference one is therefore chosen.

This basic idea was used as a starting point to develop a control-oriented methodology, where the various steps were also adapted in order to minimize the required calculation effort (i.e. the computational power requested to the on-board control unit). The methodology is based on four steps, described herein after.

Step 1: determination of the reference understeering/oversteering behavior.

Given the reference vehicle mass and the corresponding load distribution among the axle, and given a reference inflation pressure combination (i.e., a set of tire pressure values for front and rear tires), the reference understeering coefficient $K_{US,ref}$ is calculated with reference to Eq. 8 and a curvature gain vs. vehicle speed characteristic $K_{RC,ref}$ is computed with any of the methods described in Eq. 10 ($K_{RC,K,ref}$) or Eq. 11 ($K_{RC,sd,ref}$). This requires the availability of a set of tire characteristic data at least for the reference tire inflation pressure, specifically referred to the tire model currently installed on the vehicle. Several reference understeering characteristics may be computed and stored in the memory of the on-board electronic control unit, e.g. to have different reference characteristics according to different driving styles. With reference to the case of the tire and vehicle object of the present study, the reference loading condition is 1350 kg, and the reference tire inflation pressure is 2.2 bar both on the front and on the rear tires.

Step 2: determination of all the possible combinations of inflation pressures of the tires and of the related understeering/oversteering coefficient

The current vehicle mass m and its distribution, i.e. the vertical forces acting on each axle due to the vehicle loading condition, are provided as input to the algorithm, which calculates the maximum and minimum allowable tire inflation pressures for each axle. This is done by means of a look-up table which reports the iso-deflection

curves and the tire structural limits in terms of maximum tire pressure and maximum allowed vertical deflection. Once the maximum and minimum tire pressures have been calculated for each axle, i.e. ($p_{inf,F,MAX}$, $p_{inf,F,MIN}$) and ($p_{inf,R,MAX}$, $p_{inf,R,MIN}$), these intervals are divided in a number of levels, which are combined into a full-factorial matrix, in order to obtain all the possible combinations ($p_{inf,F}$, $p_{inf,R}$)$_k$. For passenger car tires, where the range between the minimum and maximum allowed pressures is typically narrow, good results can be obtained with a step of 0.1 bar.

For each combination ($p_{inf,F}$, $p_{inf,R}$)$_k$ and for the current vehicle loading condition, the understeering coefficient is computed according to Eq. 8. With reference to Eq. 7, this requires the Pacejka's coefficients PKY1 and PKY2 to be known for all the pressure levels of the ($p_{inf,F}$, $p_{inf,R}$)$_k$ combinations. As discussed above, the preferred solution is the availability of experimentally-derived tire characteristic at several tire pressures in the range of interest. In practice, it is sufficient to have the characteristics of the tires for two or three levels of pressure. For several tires that were studied at various pressures levels thanks to the availability of data from Michelin, a linear correlation was found between the parameters PKY1 and PKY2 and tire inflation pressure, as shown in Figure 14. Therefore, once the PKY coefficients are known for at least two or three inflation pressure levels, two functions PKY1=f(p_{inf}) and PKY2=f(p_{inf}) can be obtained in the form:

$$PKY(1,2)=c_{p1,(1,2)} * p_{inf}+c_{p2,(1,2)}$$ Eq.19

being the coefficients c_{p1} and c_{p2} obtained through the linear fitting of available experimentally-derived data.

Step 3: choice of the best pressure combinations among those calculated

The understeering coefficients for each possible pressure combination $K_{US,k}$, can be compared to the reference one $K_{US,ref}$. This provides a first evaluation about the eligible pressure combinations that provide a behavior similar to the reference one. A number N of pressure combinations among all the ($p_{inf,F}$, $p_{inf,R}$)$_k$ possible ones are selected (e.g., N=15), as those that minimize the parameter

$$dK_k = |K_{US,k} - K_{US,ref}|$$ Eq. 20

Figure 15 reports for the tire used in this study all the possible pressure combinations and the 15 pressure combinations which are elected for the loading conditions of Table 2, where the first case (1350 kg, 2.2 bar on both front and rear axle) is taken as a reference.

<u>Step 4: evaluation of the curvature gain curve for each of the selected tire pressure combinations and comparison with the reference one</u>

For each of the N pressure combinations ($p_{inf,F}$, $p_{inf,R}$)$_n$ obtained as result of Step 3, the curvature gain is calculated. As mentioned above, the curvature gain can be computed according to a simplified model (Eq.10) or according to the stability derivatives, preferably with the "high speed cornering" method (Eq.11), provided that the method used at this stage is the same used to evaluate the curvature gain function at reference load and pressure.

If the stability derivatives are calculated, also the Pacejka's parameters QDZ1 and QDZ2 have to be known at several inflation pressure values for the computation of the term $\left(M_{z_i}\right)_\alpha$ according to Eq. 18. Also in this case, a linear correlation between these parameters and tire pressure was highlighted from the analysis of several tires. Therefore, once the parameters QDZ1 and QDZ2 are known for at least two pressures, a linear interpolation could be performed to obtain the coefficients c_{q1} and c_{q2} and describe the two parameters in the form

$$QDZ(1,2) = c_{q1,(1,2)} * p_{inf} + c_{q2,(1,2)} \qquad \text{Eq. 21}$$

The parameters QDZ1 and QDZ2 could be then computed for any tire inflation pressure according to Eq.21.

The N curvature gain functions are then compared with the reference one (computed at Step 1). In this work, the comparison is obtained by computing for each curve a coefficient of determination,

$$R^2{}_n = \frac{\left[\sum_i\left(K_{RC,i}-\overline{K_{RC,ref}}\right)^2\right]_n}{\sum_i\left(K_{RC,ref,i}-\overline{K_{RC,ref}}\right)^2} \qquad \text{Eq. 22}$$

where the N curvature gains $K_{RC,n}$ to be analyzed are intended as "models" of the reference curvature gain $K_{RC,ref}$. Each n-th coefficient of determination provides an evaluation of the goodness of the fit obtained between the theoretical curvature gain calculated for the current vehicle mass and for the n-th tire pressure combination ($p_{inf,F}$, $p_{inf,R}$)$_n$ and the reference curvature gain, calculated at the reference loading condition and tire inflation pressure. In Eq. 22 $K_{RC,i,n}$ and $K_{RC,ref,i}$ are the i-th values of the discrete functions that describe the curvature gains $K_{RC,n}$ and $K_{RC,ref}$ as a function of the vehicle speed v.

The tire pressure combination that provides the highest coefficient of determination is chosen, as it guarantees, at the current vehicle loading conditions, an understeering characteristics as similar as possible to the reference one.
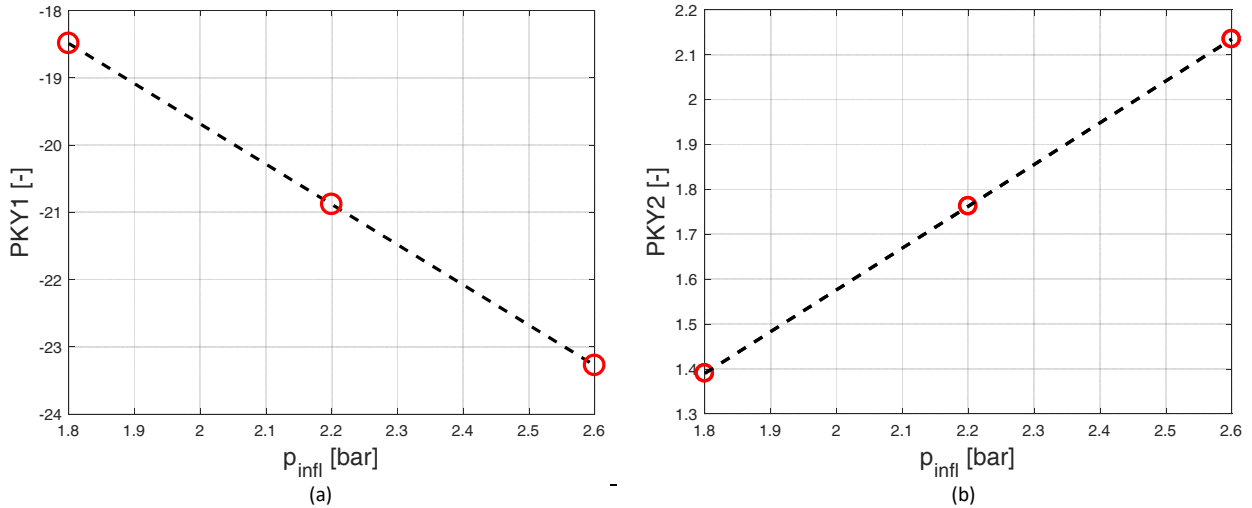
Figure 14: Coefficients PKY1 (a) and PKY2 (b), used for the calculation of the cornering stiffness according to Eq.8: dependance of these parameters on tire inflation pressure for the tire used as reference for this work.
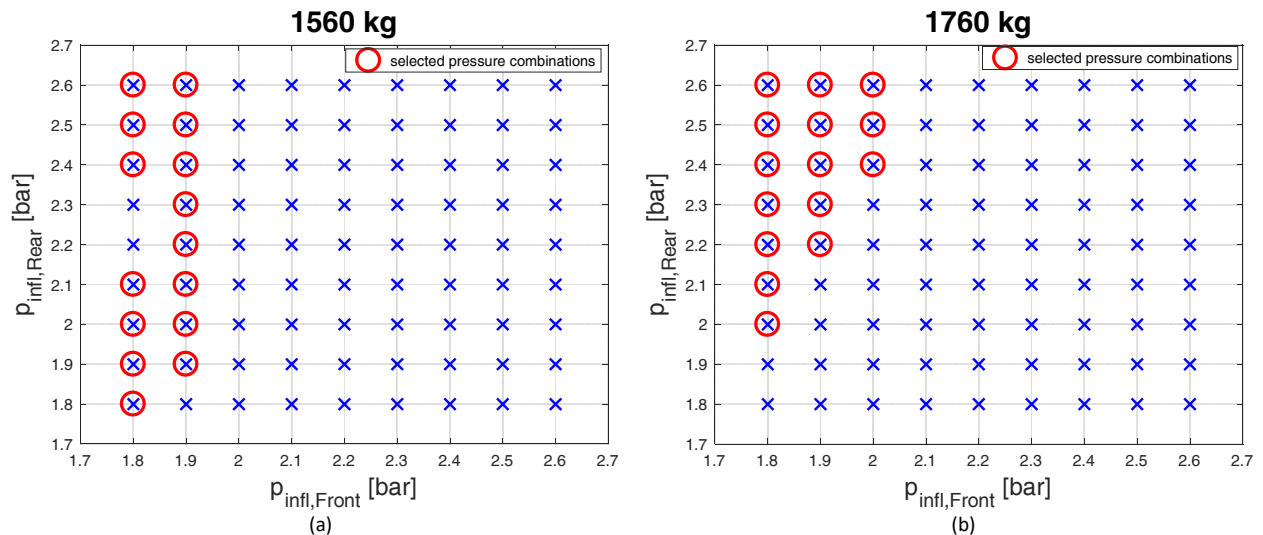

Figure 15: Selection of the eligible pressure combination for the loading case 1350 kg (a) and 1760 kg (b).

This methodology requires the knowledge of the tire characteristics according to Pacejka's MF at least for two pressure levels and the current vehicle loading conditions. The tire characterization is typically obtained through on-purpose tests performed in dedicated test facilities, therefore retrieving these data is generally expensive and time consuming for tire manufacturers. As a consequence, following the standard test methodologies, the availability of data for each tire model at several tire pressure can be limited by the additional costs that these operations would lead for tire manufacturers. Nevertheless, some studies are carried on the topic of recognizing tire characteristics directly from data acquired from on-board vehicle testing, which would make tire characterization much easier and less expensive for tires and vehicles manufacturers [39]. Therefore, tire manufacturers could provide these data to car makers for several tire models, in

order to implement a database on the vehicle ECU: when a tire set is fitted on the vehicle, the tire model is recognized by the vehicle ECU through some tire-to-vehicle communication device, and the vehicle ECU could then use the internal database to retrieve the data needed by the algorithm.

5.2 Real-time estimation of the vehicle loading conditions

Although it is out of the scope of this paper to discuss methods for the real-time estimation of the vehicle loading conditions, it is worth to highlight that several methods are discussed in the literature, which could provide this information on-board [40-45]. Some of these solutions require the installation of additional hardware, such as accelerometers to be installed inside the tire [40], while other solutions propose a software approach, as the estimation of the vehicle mass in the current working conditions can be based on some variables already available in modern vehicle ECUs, such as the speed of each wheel and, possibly, tire inflation pressure [41-45]. One software solution for the estimation of the vehicle loading conditions, i.e. total vehicle mass and its distribution among the tires, was also proposed as a side project of the current study, and its details are disclosed in [46]. The method is based on three main steps, briefly reported in the following:

1) evaluation of the total vehicle mass (m) from the apparent translating mass (m_{eq}), where the apparent vehicle mass is estimated through the dynamic equilibrium of the longitudinal forces acting on the vehicle, knowing the engine torque and speed (available in the engine ECU) and from the total resistant force, evaluated at the current tire pressure according to a calculation methodology presented in previous works [8, 11];

2) evaluation of the static vertical force on each tire by means of tire structural data, including the correlation of tire effective rolling radius to inflation pressure and vertical load, where tire pressure is known as measured by a TPMS and tire rolling radius is evaluated from wheels rotational speeds and vehicle longitudinal speed;

3) iteration of the calculation of the vertical force per each tire, in order to improve the estimation by minimizing the error between the total vehicle mass estimated at point 1 and the sum of the tire-by-tire vertical load estimated at point 2.

The method has been developed and tested in real-time in a hardware-in-the-loop environment, and it was tested by providing as input real-time data acquired on-board from the vehicle CAN during several tests on road and on track. The

tests proved that the algorithm allows the estimation of the total vehicle mass within +2.5% error, while the maximum error on the percentage vehicle load distribution is 2% (the maximum error is obtained when the real load distribution is 63% front – 37% rear and the algorithm estimates 61% front – 39% rear). The convergence time depends on the availability of suitable data on the vehicle CAN: during the tests, it was highlighted that the engine torque is often overestimated during transients, which leaded to the need for introducing plausibility logics in order to evaluate if a torque sample is acceptable for the calculation. The convergence of the algorithm was obtained in 390 valid torque samples in the best tested case.

5.3 Validation of the methodology

The described methodology has been applied to the vehicle and tire object of this study. As mentioned above, the 1350 kg load case and 2.2 bar pressure on all the tires has been assumed as reference to compute the reference understeering characteristic of the vehicle, and the remaining loading conditions reported in Table 2, i.e., 1560kg and 1760 kg, were taken as test cases to optimize tire pressure. Figure 16 reports the theoretical curvature gains calculated for the reference case, for the two test masses if no pressure control is applied (i.e., if the reference tire pressure of 2.2 bar is maintained on all the tires) and for the pressure combinations obtained as result of the methodology described above. In particular, the pressure combinations:

- 1.8 bar on the front tire and 2.4 bar on the rear tire at 1560 kg, and
- 1.8 bar on front tires and 2.6 bar on rear tires at 1760 kg

were obtained as the best fits of the reference characteristic, where the best fits were evaluated as the highest R^2 obtained from Eq.22, calculated in the vehicle speed range from 1 to 56 km/h with a step of 5 km/h. As shown in the analysis presented above, the vehicle tends to be more oversteering due to the increase of the load. At 1560 kg (Fig. 16a) the chosen pressure combination allows to obtain a characteristic very close to the reference one, thanks to the selective management of tire pressures. Nonetheless, for the second loading condition (1760 kg, Fig. 16b), it is clear that the best combination is the most understeering among all the pressure combinations allowed by the tire structural limits. As it is not possible to select lower pressure than 1.8 bar on front tires and higher pressure than 2.6 bar on rear tires, it results impossible in this case to obtain a final characteristic very close to the reference one (in this case the best fit of the reference characteristic was obtained for $R^2 = 0.23$), but still the methodology allows to individuate a pressure combination that improves the vehicle drivability providing a vehicle dynamics closer to the reference one. Figures 17 shows the same load-pressure combinations of Figure 16b, reporting the curvature gain calculated from the results of

steering pad simulations performed in Adams/Car. Although simulations show a larger difference between the reference characteristic and the final one with respect to the theoretical curvature gain of Fig. 16, it is clear that the tire pressure selected by the current methodology provides the opportunity to obtain a similar vehicle drivability at every loading condition.
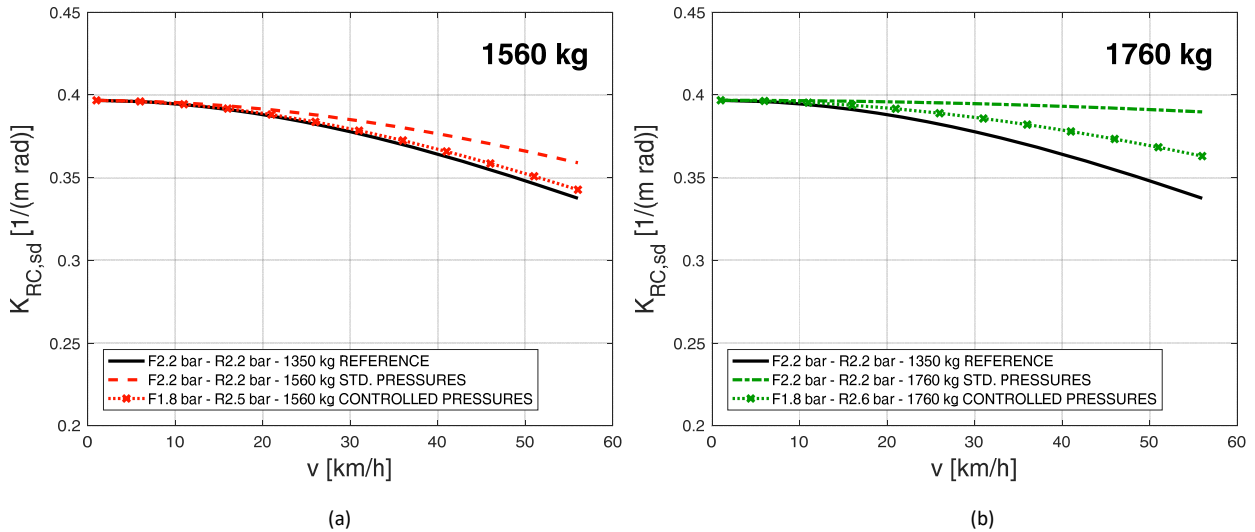

Figure 16 – Theotetical curvature gain: effect of the proposed control for the loading case 1560 kg (a) and 1760 kg (b).
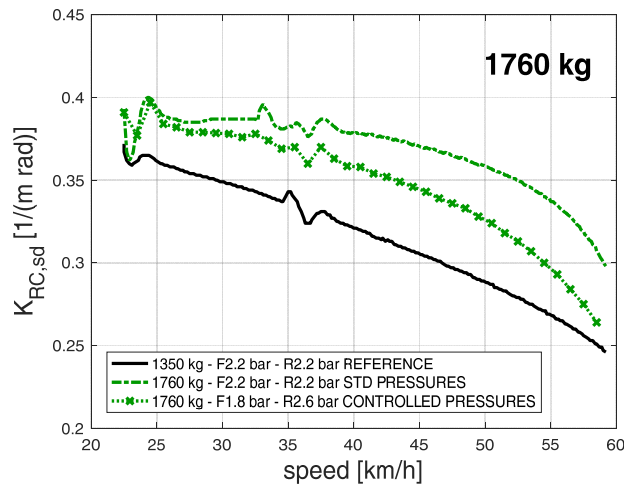

Figure 17 – Curvature gain from Adams simulations: effect of the proposed control for the loading case 1760 kg.

6. Conclusions

The effect of inflation pressure on the tire and vehicle lateral dynamics has been discussed with reference to a passenger car tire, under several loading conditions. The study includes a theoretical approach based on the calculation of the

derivatives of stabilities, as well as a multibody simulation approach. The multibody simulation model was tuned in order to fit experimental on-track test results. The main outcomes from this study are:

- The experimental steering pad tests performed at the Balocco Proving ground showed an increase of the oversteering tendency of the vehicle as tire pressure is increased, keeping tire pressure equalized on all the tires. The result was confirmed both from the multibody simulation model and from the theoretical curvature gain calculated from the derivatives of stability.

- The study of the cornering stiffness vs. vertical load characteristic at several tire inflation pressure levels highlighted as – on the tire object of this study – an increase in tire pressure at low load provides a reduction of the cornering stiffness, while the opposite occurs at high vertical load, as the characteristic shows a cross-point around 3200 N. Therefore, knowing this characteristic for a tire and the specific loading conditions of an axle, it is possible to affect the lateral vehicle dynamics by adapting tire pressure selectively on each wheel/axle.

- Both the calculation of the theoretical curvature gain and the multibody simulation showed that at low loading conditions, a reduction of the understeering tendency of the vehicle is obtained if tire pressure is increased on any of the two axles and a larger variation is obtained if pressure is varied on both of them. On the other hand, when the vehicle is loaded with a higher vertical load on the tires, an increase of tire pressure on rear tires increases the understeering tendency of the vehicle, while an increase of pressure on front tires reduces the understeering tendency of the vehicle, up to the occurrence of oversteering if the highest tire pressure is set on the front tires with the lowest tire pressure set on the rear ones.

- From the results of this investigations a control-oriented algorithm was developed. Given the tire characteristic at various tire pressure levels, and given the vehicle loading condition, the algorithm provides the best tire pressure combination able to target a specific understeering vehicle behavior. The reference understeering characteristic is defined as a target curvature gain vs. speed characteristic, and the best tire combination that provides the closest curvature gain characteristic to the target one is evaluated. The possibility to reestablish the original characteristics is anyhow limited by as minimum and maximum inflation pressure allowed by the tires of the considered application. In the reported example, the target characteristic is defined as the one obtained at the lowest vehicle load and with the nominal tire pressure level, and the target is to manage tire

pressure to achieve the same lateral dynamic behavior at every loading conditions. Nevertheless, different target characteristics could be provided according to different logics, for instance adapting the target vehicle behavior to the road conditions (dry/wet) or to the driving style (comfort/sport). The methodology is developed as part of the control logic of an intelligent system for the management of tire pressure on-board.

List of Symbols and acronyms

α	Longitudinal slip angle
β	Side slip angle of the vehicle
δ	Steering angle
$\lambda_{Ky\alpha}$	Scaling factor to account for tire-road adherence conditions
λ_t	Scale factor of peak pneumatic trail (usually equal to 1)
μ_x	Longitudinal force coefficient
μ_y	Lateral force coefficient
ρ	Density of the ambient air
σ	Longitudinal slip ratio
a_y	Lateral acceleration
$a_{y,st}$	Lateral acceleration in steady conditions
$c_{p1,(1,2)}$, $c_{p2,(1,2)}$	Fitting coefficients from the linear interpolation of $PKY1$, $PKY2$ as a function of p_{infl}
c_{px}	Tread longitudinal stiffness
$c_{q1,(1,2)}$, $c_{q2,(1,2)}$	Fitting coefficients from the linear interpolation of $QDZ1$, $QDZ2$ as a function of p_{infl}
C_α	Cornering stiffness
C_{α,M_z}	Aligning stiffness
C_σ	Longitudinal stiffness coefficient
$(C_{M_z})_\beta$	Ratio between the aerodynamic coefficient relative to the yaw moment M_z and the sideslip angle β (linearization of M_z)
$(C_y)_\beta$	Ratio between the lateral aerodynamic coefficient C_y and the vehicle sideslip angle β (linearization of C_y)
F_y	Lateral force at the tire-road interface
F_x	Longitudinal force exerted by the tire on the soil
F_z	Vertical force on the tire
F_{z0}	Reference vertical load
F,R	Front, Rear (abbreviation in graphs and underscript)
g	Gravitational acceleration

h	Half-length of the tire-road contact patch
i	Index for the i-th axle. In case of 2 axles vehicle it is also replaced by F,R
K'_i	Steering axle coefficient: $K'_i = 1$ on the steering axle, $K'_i = 0$ on non-steering ones
K_{RC}	Curvature gain (generic definition)
$K_{RC,K}$	Curvature gain evaluated from the kinematic simplified bicycle model
$K_{RC,sd}$	Curvature gain evaluated from the stability derivatives
K_{US}	Understeering coefficient
m	Vehicle total mass
m_{eq}	Equivalent, or apparent, translating vehicle mass
M_z	Self-aligning moment
$\left(M_{z_i}\right)_\alpha$	Ratio between the self-align torque M_z of the i-axle and the side slip angle α
n	Index for the n-th pressure combination
n_w	Number of wheels on an axle
N	Number or best pressure combinations selected with Step 3 of the proposed algorithm
N_β, N_r, N_δ	Derivatives of M_z with respect to the three components β, r and δ
p_{infl}	Tire inflation pressure
$PKY1, PKY2$	Experimentally-derived fitting coefficients for the cornering stiffness calculation according to the MF
$QDZ1, QDZ2$	Experimentally-derived fitting coefficients for the calculation of $\left(M_{z_i}\right)_\alpha$ according to the MF
r	Yaw angular velocity
ref	Underscript, stands for "reference"
R	Radius of a curvilinear trajectory
R^2	Coefficient of determination
R_{ul}	Unloaded tire radius
S	Frontal area of the vehicle
t	Pneumatic trail
v	Vehicle speed
v_r	Radial component of the vehicle speed
v_x	Longitudinal component of the vehicle speed

w_b Wheel-base

x_i Distance of the i-axle from the center of gravity

Y_β, Y_r, Y_δ Derivatives of F_y with respect to the three components β, r and δ

CoG Center of Gravity

ECU Electronic control unit

MF Magic Formula

References

1 Department of Transportation, National Highway Traffic Safety Administration. "Tire Pressure Monitoring Systems, Control and Displays". RIN 2127-AI33Federal Motor Vehicle Safety Standards, 49 CFR Part 571 [Docket No. NHTSA 2000-8572]. 2001

2 European Commission Directorate General Energy and Transport, "Framework Contract TREN/A1/56-2004, Lot 2: Economic assistance activities, Final Report. Cost-benefit assessment and prioritization of vehicle safety technologies (ref. TREN-ECON2-002)", 2006

3 LaClair, T.J., "Tire Rolling Resistance," in The Pneumatic Tire, Edited by J. Walter and A. Gent, University of Akron, Published by The National Highway Traffic Safety Administration, 2005

4 Michelin, "The tyre. Rolling Resistance and fuel savings", Ed. Société de Technologie Michelin, 2002

5 Genta, G. and Morello, L., "The Automotive Chassis. Volume 1: Components Design", Mechanical Engineering Series, Springer, 2009

6 Calwell, C., Ton, M., Gordon, D., Reeder, T., Olson, M. and Foster, S., "California state fuel-efficient tire report: Volume II", California Energy Commission, January 2003

7 Reithmaier W., Salzinger T., "Survey on moto vehicle tyres & related aspects – Final report", prepared by TUV Automotive GmbH, commissioned by The European Commission Enterprise Directorate General, 2003

8   d'Ambrosio, S., Vitolo, R., "Potential impact of active tire pressure management on fuel consumption reduction in passenger vehicles", Proceedings of the IMechE, Part D: Journal of Automobile Engineering, 233(4):961-975, 2019, https://doi.org/10.1177/0954407018756776

9   d'Ambrosio, S., Mameli, E., Vitolo, R., "Impact assessment of an intelligent central tire inflation system for passenger cars", 7th Transport Research Arena TRA 2018, April 16-19, Vienna, Austria, 2018. https://doi.org/10.5281/zenodo.1486718

10 d'Ambrosio, S., Oliva, E., Salamone, N., and Vitolo, R., "Active Tire Pressure Control (ATPC) for Passenger Cars: Design, Performance, and Analysis of the Potential Fuel Economy Improvement," SAE Int. J. Passeng. Cars – Mech. Syst.11(4):321-339, 2018, https://doi.org/10.4271/2018-01-1340

11 d'Ambrosio, S., Mameli, E., Vitolo, R., Calaon, I. et al., "Fuel Consumption Reduction on Heavy-Duty and Light-Duty Commercial Vehicles by Means of Advanced Central Tire Inflation Systems", SAE Int. J. Commer. Veh. 11(5):267-289, 2018, https://doi.org/10.4271/2018-01-1334

12 Kole, P.J., Lohr, A.J., Van Belleghem, F.G.A.J., and Ragas, A.M., "Wear and Tear of Tyres: A Stealthy Source of Microplastics in the Environment", Int. J. Environ. Res. Public Health 2017, 14, 1265; doi:10.3390/ijerph14101265

13 Hooftman, N., Messagie1, M., Van Mierlo, J., and Coosemans, T., "A review of the European passenger car regulations – Real driving emissions vs local air quality", Renewable and Sustainable Energy Reviews 86 (2018) 1–21, https://doi.org/10.1016/j.rser.2018.01.012

14 Thorpe, A, and Harrison, R.M., "Sources and properties of non-exhaust particulate matter from road traffic: A review", Science of the total environment 400 (2008) 270 – 282, https://doi.org/10.1016/j.scitotenv.2008.06.007.

15 Grigoratos, T. and Martini, G., "Non-exhaust traffic related emissions – Brake and tyre wear PM", EUR - Scientific and Technical Research Reports, Publications Office of the European Union (2014), https://doi.org/10.2790/21481.

16 Timmers, V.R.J.H., and Achten, P.A.J., "Non-exhaust PM emissions from electric vehicles", Atmospheric Environment 134 (2016) 10-17, http://dx.doi.org/10.1016/j.atmosenv.2016.03.017.

17 European Commission, Staff working Document, SEC(2008)1908 (23.05.2008.), Annex to the Regulation of the European Parliament and of the Council concerning Type-approval requirements for the general impact asessmentEuropean Parliament, "Regulation (EC) No 443/2009 of the European Parliament and of the Council of

23 April 2009 setting emission performance standards for new passenger cars as part of the Community's integrated approach to reduce CO 2 emissions from light-duty vehicles." Official Journal of the European Union, L140/1. 5 June, 2009

18 U.S. 106th Congress. "Transportation Recall Enhancement, Accountability and Documentation (TREAD) Act." Public Law 106-414-Nov. 1, 2000

19 Transport&Environment, "Failuer of Inirect Tire Pressure monitoring systems puts drivers and road users at risk", report on independet tests, November 2016

20 Pacejka, H. B., "Tyre and Vehicle Dynamics", Butterworth-Heinemann, 2002

21 Besselink, I.J.M., Schmeitz, A.J.C., Pacejka, H.B., "An improved Magic Formula/Swift tire model that can handle inflation pressure changes", Vehicle System Dynamics 2010, 48 (1) pp337-352, Taylor & Francis Ltd

22 Millar, P., Woodward, D., Friel, S., Woodside, A., "An investigation of the variation of contact area with inflation pressure" , 5th International Conference Bituminous Mixtures and Pavements, 2011

23 Ivanov, V., "Analysis of Tire Contact Parameters Using Visual Processing", Advances in tribology 2010, Hindawi Publishing Corporation (doi: 10.1155/2010/491723)

24 Schmeitz, A.J.C., Besselink, I.J.M., Hoogh, de, J. & Nijmeijer, H. (2005). Extending the Magic Formula and SWIFT tyre models for inflation pressure changes. Reifen, Fahrwerk, Fahrbahn (pp. 201-225). Germany, Hannover: Technische Universiteit Eindhoven.

25 Rievaj, V., Vrabel, J. and Hudak, A., "Tire Inflation Pressure Influence on a Vehicle Stopping distances", International Journal of Traffic and Transportation Engineering 2013, 2 (2) pp 9-13, Scientific and Academic Publishing

26 Reiter, M. and Wagner, J., "Automated Automotive Tire Inflation System – Effect of Tire Pressure on Vehicle Handling", 6th IFAC Symposium Advances in Automotive Control, 2010

27 Vitolo, R., d'Ambrosio, S., Salamone, N., et al., "On-board centralized system for regulating the pressure of tyres of a motor vehicle", Patent Application WO 2017/089915 A1. 24 Nov. 2015.

28 Vitolo, R., d'Ambrosio, S., Salamone, N., et al., "On-board centralized system for regulating the pressure of tyres of a motor vehicle", Patent application WO2017/089916 A1. 24 Nov. 2015.

29 Vitolo, R., d'Ambrosio, S., De Mattei, E., "Apparatus and method for computing tire pressures", Italian Patent application 102017000128722. November 10th, 2017.

30 Genta, G., Morello, L., "The Automotive Chassis – Vol. 2: Component design", Springer, 2009

31 Fancher, P. S. (Ed.) "Descriptive parameters used in analysing the braking and handling of heavy trucks"– measurements of the longitudinal and lateral traction properties of truck tyres, vol. 3, Data volume III (Notebook III). Final report UM-HSRI-81-19-3-4, University of Michigan, Highway Safety Research Institute, 1981, pp. 357–373.

32 M K Al-Solihat, S Rakheja, and A K W Ahmed – "Influence of tyre pressure on an urban bus transient and steady state handling performance" - Proceedings of the Institution of Mechanical Engineers, Part D: Journal of Automobile Engineering, vol. 224, no. 7, pp. 893-908, 2010.

33 Seymour, S., and Pivonka, D., "Active Tire Controller Device", U.S. Patent No. 2012/0221196 A1. 30 Aug. 2012.

34 Villella, M.G., Gaffney, E.F., "Closed loop vehicle dynamic control for use with yaw rate controllers", U.S. Patent No. 7308353 B2. 11 Dec. 2007

35 Fennel, H., Batistic, I., "Method of controlling the performance of a motor vehicle", U.S. Patent No. 6616250 B1. 9 Sept. 2003

36 Gronau, R., Woywod, J., "Method for regulating the handling of a vehicle", U.S. Patent Application No. 2006/0108863. 25 May 2006.

37 van Zanten, A., Nimmo, M., Stams, M., Pineau, J., Gauthier, P., "Optimization of a vehicle dynamics control using tire information", U.S. Patent Application No. 2007/0112477. 17 May 2007.

38 Muthukumar, P., "Smart active tyre pressure optimising system", U.S. Patent Application No. 2015/005982. 1 Jan. 2015.

39 Van Gennip, M., and McPhee, J., "Parameter Identification and Validation for Combined Slip Tire Models Using a Vehicle Measurement System", SAE Int. J. Veh. Dyn., Stab., and NVH 2(4):297-310, 2018, https://doi-org /10.4271/2018-01-1339.

40 Brusarosco, M., Mancosu, F., Arosio, D., "Method and system for determining a tyre load during the running of a motor vehicle", U.S. Patent No. US 8,874,386 B2. 28 Oct. 2014.

41 Chaklader, A.C.D., "Vehicle weight and cargo load determination using tire pressure", U.S. Patent No. US 6,449,582 B1, 10 Sept. 2002.

42 Keller, L., Griesser, M., Köbe, A., Säger, P., "Method for determining the load exerted on a vehicle tire", U.S. Patent No. US 7,013,721 B2. 21 Mar. 2006.

43 Elliott, J.A., Fulmer, B.T., "Method for determining axle load of a moving vehicle", U.S. Patent No. US 6,688,168 B1. 10 Feb. 2004.

44 Katou, M., "Vehicle load weight detecting apparatus", U.S. Patent No. US 8,096,174 B2. 17 Jan. 2012.

45 Singh, K.B., Fenkanyn, J.M., Patel, A., et. al., "Vehicle tire load estimation", European Patent EP 2,722,202 A1. 23 Apr. 2014.

46 Vitolo, R., d'Ambrosio, S., Vigna, L.F., et al., "Apparatus and method for estimating loading conditions of tires", Italian Patent application 102018000005764, May 28th, 2018.

47 ISO 4138:2112, "Passenger cars – Steady-state circular driving behavior – Open-loop test methods".

48 Sina, N., Yazdi, M.R.H., Esfahanian, V., "A novel method to improve vehicle energy efficiency: Minimization of tire power loss", Proceedings of the IMechE, Part D: Journal of Automobile Engineering, 234(4):1153-1166, 2020, https:// doi.org/10.1177/0954407019861241.

49 Höpping, K. and Augsburg, K., "Dynamic tire pressure control system - analysis of the effect to longitudinal vehicle dynamics and fuel consumption", Shaping the future by engineering : 58th IWK, Ilmenau Scientific Colloquium, Ilmenau, Germany, September 8-12, 2014.

50 Augsburg, K., Ivanov, V.; Kruchkova, K., Höpping, K. et al., "Project Adtyre: towards dynamic tyre inflation control", Proceedings of the FISITA 2012 World Automotive Congress. Lecture notes in Electrical Engineering, Vol. 198. 185-198, 2013, doi: 10.1007/978-3-642-33795-6_16.